

Measurement of Higgs Production Cross Section via Vector Boson Fusion in $H \rightarrow ZZ \rightarrow 4l$ final state at 13 TeV using Artificial Neural Networks

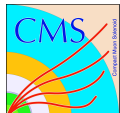
Miquéias Melo de Almeida¹

Advisor: Andre Sznajder¹
Co-advisor: Nicola De Filippis²

¹Universidade do Estado do Rio de Janeiro

²INFN and Politecnico di Bari

April 28th, 2019



1 CMS AN-18-120

- Introduction
- Theoretical Motivation
- The CMS Experiment at CERN
- Datasets, Triggers and Simulated Samples
- Objects Selections
- Event Selections
- Signal and Background Estimation
- Artificial Neural Networks (ANNs)
- Systematic Uncertainties
- Statistical Analysis and Results

2 CMS L1 Tracking Trigger AM+FPGA

- Introduction
- Hardware Work
- Simulation Studies

3 The Fast Matrix Element (FastME)

- Introduction
- Simulation Studies
- The FastME Package

4 Conclusions

The CMS AN-18-120

Introduction

- This analysis aims an isolated measurement of the Higgs VBF production XS through the HZZ4L channel via ANN discriminants;

- Analysis summary:

- follows similar requirements established in CMS HZZ4L analysis;
- VBF signal region (VBF-SR) defined similarly to CMS VBF category (no MELA);
- proposes the usage of a 3rd jet when available;
- events at VBF-SR divided into two jet-based subcategories;
- Artificial Neural Network (ANN) as a VBF discriminant;

Documentation

Available on the CMS information server

CMS AN-18-120

CMS Draft Analysis Note

The content of this note is intended for CMS internal use and distribution only

2018/11/29
 Head Id: 482729
 Archive Id: 479138:482729MP
 Archive Date: 2018/11/28
 Archive Tag: trunk

Measurement of Higgs Production Cross Section via Vector Boson Fusion in $H \rightarrow ZZ \rightarrow 4l$ final state at 13 TeV using Artificial Neural Networks

M. M. Almeida¹, A. Sznajder¹, N. De Filippis², P. Bhat³, S. Uzunyan⁴, M. Eads⁴, D. Faia⁴, R. Singh⁴, H. Prosper⁵, and K. Johnson⁵

¹Universidade do Estado do Rio de Janeiro

²INFN and Politecnico di Bari

³Fermi National Accelerator Laboratory

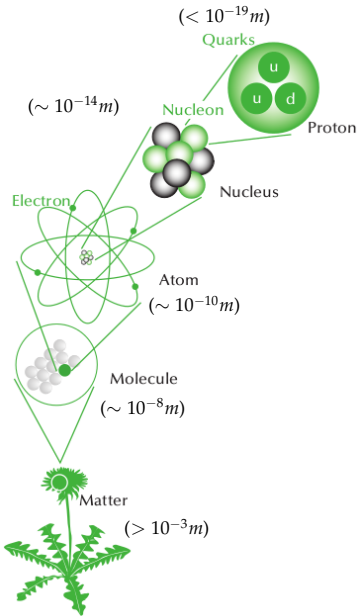
⁴Northern Illinois University

⁵Florida State University

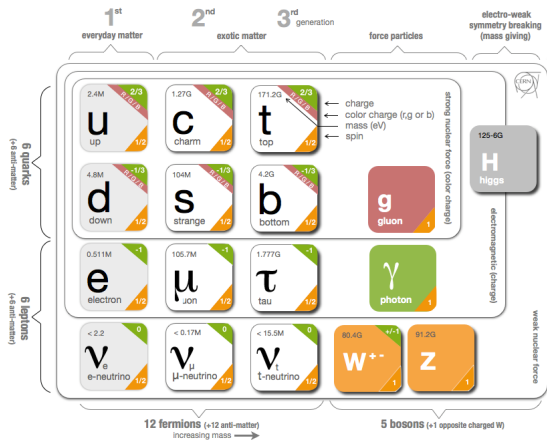
Abstract

A isolated measurement of the Higgs boson production cross section in the Vector Boson Fusion (VBF) production mode is performed in the $H \rightarrow ZZ \rightarrow 4l(l = e, \mu)$ channel. The study is performed using data samples corresponding to an integrated luminosity of 35.9 fb^{-1} from pp collisions at $\sqrt{s} = 13 \text{ TeV}$, which has been collected by the CMS experiment during 2016 at the LHC. A multivariate analysis is performed through the usage of Artificial Neural Networks (ANNs). Statistical shape analysis of ANNs developed for two orthogonal jet-based categories is done by combining the discriminants distribution from each category. The Higgs VBF signal strength modifier is measured to be $\mu_{qqlj}^{obs} = 1.28^{+1.34}_{-0.88}$ for a expected Higgs boson of $m_H = 125 \text{ GeV}$. This result is comparable with the SM expectation. The observed significance of the present analysis is $\sigma_{qqlj}^{obs} = 1.9$, while the expected one is $\sigma_{qqlj}^{exp} = 1.8$. The observed and expected 95%CL limits are estimated as $\mu_{qqlj}^{exp} < 3.79$ and $\mu_{qqlj}^{exp} < 1.66$, respectively. A projection for future luminosities is also presented and it is expected that the present analysis will have enough significance for the VBF-Higgs production evidence (3.4σ) at 150 fb^{-1} and the observance (5.1σ) at 359 fb^{-1} .

Particle Physics and the Standard Model



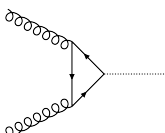
- Elementary Particle Physics is the field of Physics dedicated to the study of fundamental building blocks of matter and their interactions;
- The Standard Model (SM) resumes what physicists know so far:



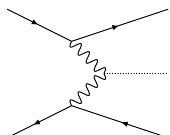
The Higgs Boson

- In Physics symmetry is a strong basic property: the theory must be invariant under change of frame;
- Particle interactions rise due to symmetry in Quantum Physics. However, symmetry brings a trouble: particles should not have mass!
- This is a clear contrast to what we see in the nature (we have mass);
- Solution: a new particle which interacts with other particles (and itself) giving their mass. This particle is the Higgs boson observed in 2012:

$$gg \rightarrow H$$



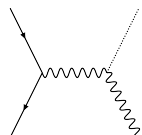
$$q\bar{q} \rightarrow H q\bar{q}$$



fusion of gluons

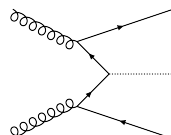
fusion of bosons Z/W
(VBF)

$$q\bar{q} \rightarrow VH$$

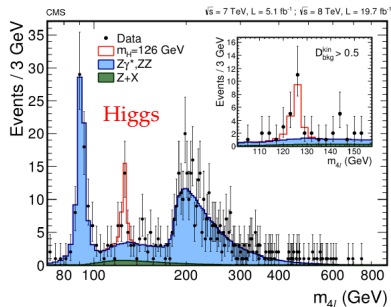


radiation from Z/W

$$gg \rightarrow t\bar{t}H$$



fusion of top quarks

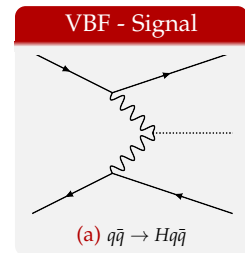


- The Higgs can appear through some interactions of the elementary particles, such as:

Physics Processes in this Analysis

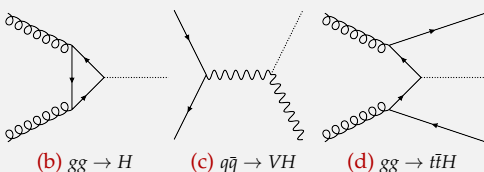
- Search for Higgs produced via Vector Boson Fusion (VBF):

- second largest Higgs production mode;
- tree-level and clean of beyond-SM processes;
- good frame for measurements of Higgs properties;
- based on reconstruction of four isolated leptons + at least two jets;

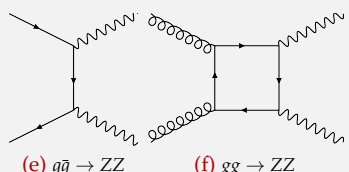


- Expected backgrounds:

SM Higgs Production Modes - Backgrounds

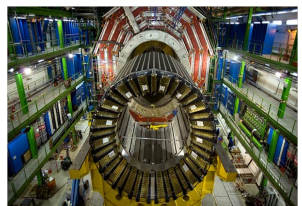
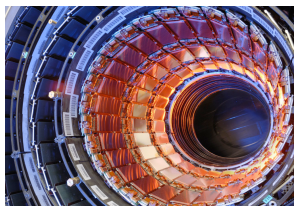
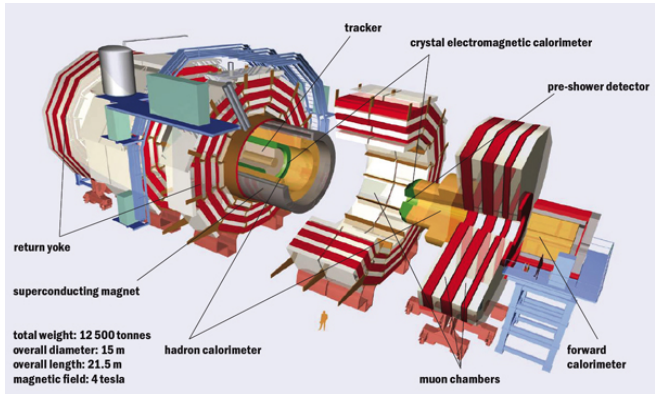


SM Backgrounds



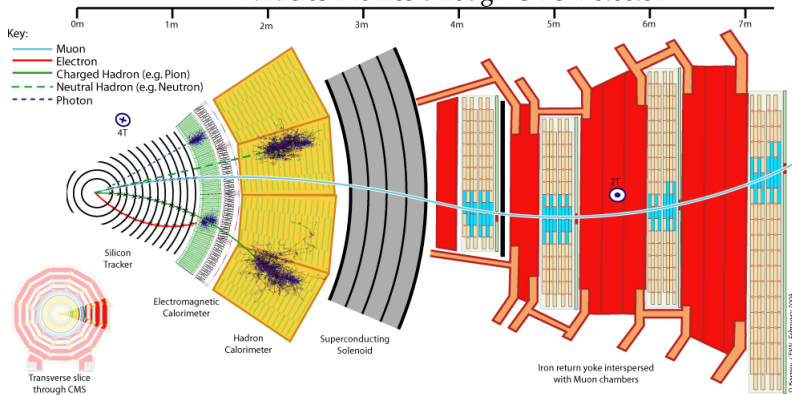
- Additionally there is the $Z + X$ derived via *data-driven* method;

Compact Muon Solenoid in a Nutshell



CMS-Particles Interaction Profile

Particles Profiles through CMS Detector



- CMS has particle-specialized sub-detectors;
- "Long-life" particles (reach detectors) are identified by patterns from the sub-detectors;
- "Short-life" particles (decay into other particles before reach a detector) are accessed through the properties of "long-life" particles;

Datasets and Triggers

- Data:

- full 2016 Data: $L = 35.9\text{fb}^{-1}$, 03Feb ReReco (full list in backup);
- JSON: Cert_271036_284044_13TeV_23Sep2016ReReco_Collisions16_JSON.txt.

- Triggers:

- based on multi-lepton HLT paths;
- isolated di-lepton paths + non-isolated tri-lepton paths + single-lepton paths;
- requirements to avoid double-counting is applied;
- overall trigger efficiency is higher than 99% wrt. 4-lepton analysis selection;

| HLT path | L1 seed | Prescale | Primary dataset |
|---|---------------------|----------|-----------------|
| HLT_Ele17_Ele12_CaloIdL_TrackIdL_IsoVL_DZ | L1_DoubleEG_15_10 | 1 | DoubleEG |
| HLT_Ele23_Ele12_CaloIdL_TrackIdL_IsoVL_DZ | L1_DoubleEG_22_10 | 1 | DoubleEG |
| HLT_DoubleEle33_CaloIdL_GsfTrkIdVL | (Multiple) | 1 | DoubleEG |
| HLT_Ele16_Ele12_Ele8_CaloIdL_TrackIdL | L1_TripleEG_14_10_8 | 1 | DoubleEG |
| HLT_Mu17_TrkIsoVVL_Mu8_TrkIsoVVL | L1_DoubleMu_11_4 | 1 | DoubleMuon |
| HLT_Mu17_TrkIsoVVL_TkMu8_TrkIsoVVL | L1_DoubleMu_11_4 | 1 | DoubleMuon |
| HLT_TripleMu_12_10_5 | L1_TripleMu_5_5_3 | 1 | DoubleMuon |
| HLT_Mu8_TrkIsoVVL_Ele17_CaloIdL_TrackIdL_IsoVL | L1_Mu5_EG15 | 1 | MuonEG |
| HLT_Mu8_TrkIsoVVL_Ele23_CaloIdL_TrackIdL_IsoVL | L1_Mu5_EG20 | 1 | MuonEG |
| HLT_Mu17_TrkIsoVVL_Ele12_CaloIdL_TrackIdL_IsoVL | L1_Mu12_EG10 | 1 | MuonEG |
| HLT_Mu23_TrkIsoVVL_Ele12_CaloIdL_TrackIdL_IsoVL | L1_Mu20_EG10 | 1 | MuonEG |
| HLT_Mu23_TrkIsoVVL_Ele8_CaloIdL_TrackIdL_IsoVL | L1_SingleMu* | 1 | MuonEG |
| HLT_Mu8_DiEle12_CaloIdL_TrackIdL | L1_Mu6_DoubleEG10 | 1 | MuonEG |
| HLT_DiMu9_Ele9_CaloIdL_TrackIdL | L1_DoubleMu7_EG7 | 1 | MuonEG |
| HLT_Ele25_eta2p1_WPTight | L1_SingleEG* | 1 | SingleElectron |
| HLT_Ele27_WPTight | L1_SingleEG* | 1 | SingleElectron |
| HLT_Ele27_eta2p1_WPLoose_Gsf | L1_SingleEG* | 1 | SingleElectron |
| HLT_IsoMu20 OR HLT_IsoTkMu20 | L1_SingleMu* | 1 | SingleMuon |
| HLT_IsoMu22 OR HLT_IsoTkMu22 | L1_SingleMu* | 1 | SingleMuon |

Simulated Samples

- Signal: VBF_HToZZTo4L_M125_13TeV_powheg2_JHUGenV6_pythia8;
- Background: remaining samples in the table;
- Special samples for ggH (*) and qqZZ (**) included.

| Process | Dataset Name | $\sigma \cdot BR (fb)$ |
|---|---|--------------------------|
| SM Higgs MC Samples | | |
| * $gg \rightarrow H \rightarrow ZZ \rightarrow 4l$ | [1] GluGluHToZZTo4L_M125_13TeV_powheg2_minloHJJ_JHUGenV6_pythia8 | 12.180 |
| $q\bar{q} \rightarrow H q\bar{q} \rightarrow ZZ q\bar{q} \rightarrow 4l q\bar{q}$ | [1] VBF_HToZZTo4L_M125_13TeV_powheg2_JHUGenV6_pythia8 | 1.044 |
| $q\bar{q} \rightarrow W^+ H \rightarrow W^+ ZZ \rightarrow 4l + X$ | [1] WplusH_HToZZTo4L_M125_13TeV_powheg2-minlo-HWJ_JHUGenV6_pythia8 | 0.232 |
| $q\bar{q} \rightarrow W^- H \rightarrow W^- ZZ \rightarrow 4l + X$ | [1] WminusH_HToZZTo4L_M125_13TeV_powheg2-minlo-HWJ_JHUGenV6_pythia8 | 0.147 |
| $q\bar{q} \rightarrow ZH \rightarrow ZZZ \rightarrow 4l + X$ | [1] ZH_HToZZ_4LFilter_M125_13TeV_powheg2-minlo-HZJ_JHUGenV6_pythia8 | 0.668 |
| $gg \rightarrow t\bar{t}H \rightarrow t\bar{t}ZZ \rightarrow 4l + X$ | [1] ttH_HToZZ_4LFilter_M125_13TeV_powheg_JHUGen_pythia8 | 0.393 |
| $gg \rightarrow H \rightarrow WW \rightarrow 2l2v$ | [1] GluGluHToWWTo2L2Nu_M125_13TeV_powheg_JHUGen_pythia8 | 1101.790 |
| $q\bar{q} \rightarrow H q\bar{q} \rightarrow WW q\bar{q} \rightarrow 2l2v$ | [1] VBFHToWWTo2L2Nu_M125_13TeV_powheg_JHUGen_pythia8 | 85.776 |
| $q\bar{q} \rightarrow W^+ H \rightarrow W^+ WW \rightarrow l\nu 2l2v$ | [1] HWplusJ_HToWWTo2L2Nu_WToLNu_M125_13TeV_powheg_pythia8 | 2.138 |
| $q\bar{q} \rightarrow W^- H \rightarrow W^- WW \rightarrow l\nu 2l2v$ | [1] HWminusJ_HToWWTo2L2Nu_WToLNu_M125_13TeV_powheg_pythia8 | 1.357 |
| $q\bar{q} \rightarrow ZH \rightarrow ZWW \rightarrow 2l2l2v$ | [1] HZJ_HToWWTo2L2Nu_ZTo2L_M125_13TeV_powheg_pythia8 | 2.029 |
| $gg \rightarrow b\bar{b}H \rightarrow b\bar{b}WW \rightarrow 2l2v + X$ | [1] bbHToWWTo2L2Nu_M-125.4FS_yb2_13TeV_amcatnlo | 11.068 |
| SM Backgrounds MC Samples | | |
| $q\bar{q} \rightarrow ZZ \rightarrow 4l$ | [1] ZZTo4L_13TeV_powheg_pythia8 | 1256.000 |
| $q\bar{q} \rightarrow ZZ \rightarrow 4l$ | [1] ZZTo4L_13TeV_amcatnlo_FXFX_pythia8 | 1212.000 |
| * * $q\bar{q} \rightarrow ZZ \rightarrow 4l + jets (EWK)$ | [1] ZZJJTo4L_EWK_13TeV-madgraph_pythia8/ | 4.404 |
| $gg \rightarrow ZZ \rightarrow 4e$ | [1] GluGluToContinToZZTo4e_13TeV_MCFM701 | 1.590 |
| $gg \rightarrow ZZ \rightarrow 4\mu$ | [1] GluGluToContinToZZTo4mu_13TeV_MCFM701 | 1.590 |
| $gg \rightarrow ZZ \rightarrow 4\tau$ | [1] GluGluToContinToZZTo4tau_13TeV_MCFM701 | 1.590 |
| $gg \rightarrow ZZ \rightarrow 2e2\mu$ | [1] GluGluToContinToZZTo2e2mu_13TeV_MCFM701 | 3.190 |
| $gg \rightarrow ZZ \rightarrow 2e2\tau$ | [1] GluGluToContinToZZTo2e2tau_13TeV_MCFM701 | 3.190 |
| $gg \rightarrow ZZ \rightarrow 2\mu2\tau$ | [1] GluGluToContinToZZTo2mu2tau_13TeV_MCFM701 | 3.190 |
| $Z \rightarrow ll + jets$ | [1] DYJetsToLL_M-10to50TuneCUETP8M1_13TeV-amcatnloFXFX_pythia8 [1] DYJetsToLL_M-50_TuneCUETP8M1_13TeV-amcatnloFXFX_pythia8 | $6.104e^6$ $1.861e^7$ |
| $t\bar{t}$ | [1] TTJets_TuneCUETP8M1_13TeV-amcatnloFXFX_pythia8 | $815.96e^3$ |
| $t\bar{t} \rightarrow 2l2v2b$ | [1] TTTTo2L2Nu_13TeV_powheg | $8.731e^4$ |
| $WZ \rightarrow 3l\nu$ | [1] WZTo3LNu_TuneCUETP8M1_13TeV_powheg_pythia8 | 4430 |
| ZZZ | [1] ZZZ_TuneCUETP8M1_13TeV-amcatnlo_pythia8 | 13.980 |
| WWZ | [1] WWZ_TuneCUETP8M1_13TeV-amcatnlo_pythia8 | 165.100 |
| WZZ | [1] WZZ_TuneCUETP8M1_13TeV-amcatnlo_pythia8 | 55.650 |
| $t\bar{t}W$ | [1] TTWJetsToLNu_TuneCUETP8M1_13TeV-amcatnloFXFX-madspin_pythia8 | 204.300 |
| $t\bar{t}Z$ | [1] TTZToLLNuNu_M-10_TuneCUETP8M1_13TeV-amcatnlo_pythia8 | 252.900 |

[1] RunII Summer16 MiniAOD v2 - PU Moriond17_80X_mcRun2_asymptotic_2016_TrancheIV_v6-v1/

Objects Selections

Electrons (momentum calibration applied)

Loose

- $p_T > 7 \text{ GeV};$
- $|\eta| < 2.5;$
- $|d_{xy}| < 0.5 \text{ cm};$
- $|d_z| < 1.0 \text{ cm}.$

Tight

- Loose selections plus:
 - $|SIP_{3D}| < 4.0;$
 - Isolation ($\Delta R = 0.3$) $< 0.35;$
 - MVA (BDT) calorimeter-based:

| Minimum BDT score | $ \eta < 0.8$ | $0.8 < \eta < 1.479$ | $ \eta > 1.479$ |
|----------------------------|----------------|------------------------|------------------|
| $5 < p_T < 10 \text{ GeV}$ | -0.211 | -0.396 | -0.215 |
| $p_T > 10 \text{ GeV}$ | -0.870 | -0.838 | -0.763 |

Muons (momentum calibration and FSR applied)

Loose

- Global/Tracker Muons;
- $p_T > 5 \text{ GeV};$
- $|\eta| < 2.4;$
- $|d_{xy}| < 0.5 \text{ cm};$
- $|d_z| < 1.0 \text{ cm}.$

Tight

- Loose selections plus:
 - PF Muon;
 - $|SIP_{3D}| < 4.0;$
 - Isolation ($\Delta R = 0.3$) $< 0.35;$
 - Ghost-cleaning (single- μ as more).

Objects Selections

Photons and FSR

- $p_T > 2 \text{ GeV}$, $|\eta| < 2.4$;
- Isolation ($\Delta R = 0.3$) < 1.8 ;
- $\Delta R(\gamma, l)/E_{T,\gamma}^2 \geq 0.012$ and $\Delta R(\gamma, l) \geq 0.5$;

Jets (JECs applied)

- anti-kT ($R = 0.4$) PF CHS (*Carged Hadron Subtracted*) jets;
- $p_T > 30 \text{ GeV}$, $|\eta| < 4.7$;
- cleaning $\Delta R(jet, l/\gamma) > 0.4$;
- b-tagging with CSV (*Combined Secondary Vertex*) algorithm;

MET (*Missing Transverse Energy*)

- PF MET with type-1 correction: $\vec{E}_T^{miss} = -(\sum_{jets} \vec{p}_T^{JEC} + \sum_{uncl.} \vec{p}_T)$;
- filters^a from JETMET POG applied (improves signal-to-noise ratio).

^aSee backup slides.

Event Selections

SM Higgs

- 1 Z candidates:** pair of same-flavor, opposite-charge and FSR corrected leptons (e^+e^- , $\mu^+\mu^-$) having invariant mass $12 < m_{ll(\gamma)} < 120$ GeV;
- 2 ZZ candidates:** pair of non-overlapping (different leptons) Z candidates. The Z with smallest $|m_{ll(\gamma)} - m_Z^{PDG}|$ is identified as Z_1 and the other Z as Z_2 . ZZ candidates must satisfy:
 - any two leptons must have $\Delta R(\eta, \phi) > 0.02$ (**ghost removal**);
 - at least two out of the four leptons must have $p_T > 10$ and 20 GeV;
 - any two leptons must have (without FSR- γ) $m_{ll} > 4$ GeV (**QCD suppression**);
 - $m_{Z_1} > 40$ GeV and $m_{Z_1Z_2} > 100$ GeV;
 - if more than one ZZ candidate survives previous cuts, the one with highest scalar leptons p_T sum is chosen;



VBF Signal Region (VBF-SR)

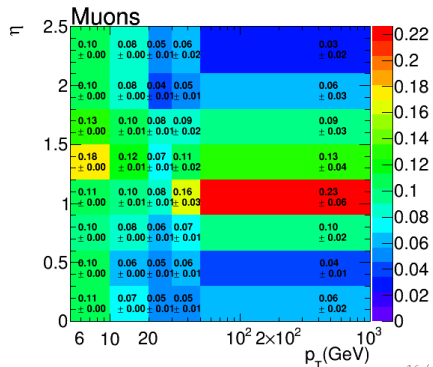
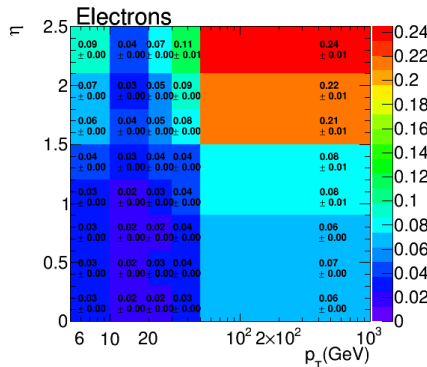
- 3** In order to enhance VBF-to-background ratio:
 - Number of jets:
 - EITHER, 2 or 3 jets from which at most one b-tagged jet;
 - OR, more than 3 jets with no b-tagged jet;
 - ZZ candidates must have $118 \leq m_{Z_1Z_2} \leq 130$ GeV;

Signal and Background Estimation

- In this analysis the background at the VBF-SR is composed by:
 - remaining Higgs production modes (ggH , VH and ttH);
 - SM backgrounds ($qqZZ$, $ggZZ$ and $Z + X$);
- The Higgs production modes (including VBF) are estimated from MC normalized by proper $\sigma.BR$ given by LHC Higgs XS Working Group computation;
- The SM backgrounds $qqZZ$ and $ggZZ$ are modeled from MC and properly applying scale factors accounting for NLO and NNLO corrections, as done for the SM Higgs analysis;
- The SM background $Z + X$ is estimated from Data via the *data-driven* Fake Rate (FR) method;

Z + X Background Estimation

- Originates from processes with non-prompt leptons: heavy-flavor meson decays, mis-reconstructed jets and electrons from γ conversions;
- Strategy: measure FR in specific control regions (CRs) and apply it to the SR;
- First step, measuring the FR:
 - samples of $Z l_1 l_2 + l_3$ ($l_{1,2}$ tight leptons, l_3 loose lepton);
 - $p_T^{l_1, l_2} > 10, 20$ GeV, $m_{l_1 l_2} < 4$ GeV, $|m_{l_1 l_2} - m_Z^{\text{PDG}}| < 7$ GeV and $E_T^{\text{miss}} < 25$ GeV;
 - contribution from WZ (with potential 3 real leptons) is subtracted;
- The FR ($N_{\text{tight}} / N_{\text{loose}}$, ie. probability of loose lepton pass tight selections) is mapped wrt. to $p_T^{l_3}$ vs. η^{l_3} :

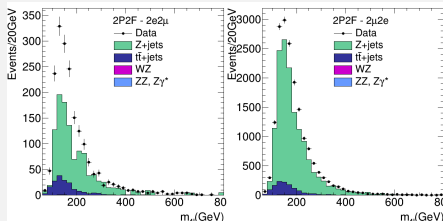
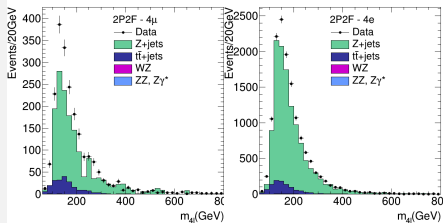


Z + X Background Estimation

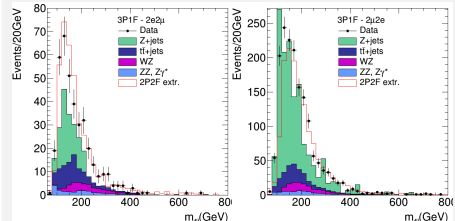
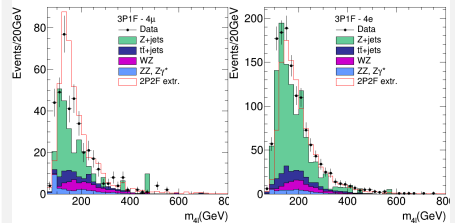
- Second step, building CRs:

- Orthogonal to the SM Higgs selections and enriched by fake-lepton events;
- Require $Z_{l_1 l_2} Z_{l_3 l_4}$ where $l_{1,2}$ are always *tight* leptons and if $l_{3,4}$ are *loose* leptons, define 2P2F while if only l_4 is *loose*, define 3P1F;

$$2\text{P2F CR: } w_{Data} = \frac{f_3}{1-f_3} + \frac{f_4}{1-f_4}$$



$$3\text{P1F CR: } w_{Data} = \frac{f_4}{1-f_4}$$

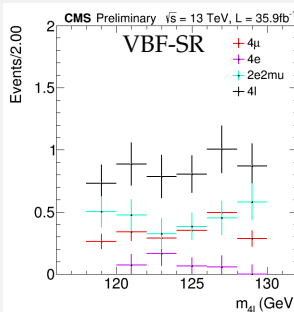
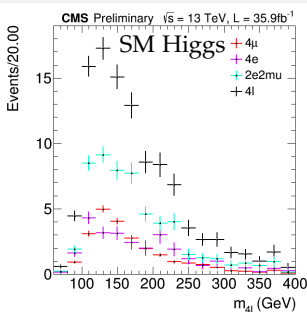


Z + X Background Estimation

- Third step, using the measured FR(p_T, η) in order to estimate Z + X yield and shape in the SR;
- At SR, Z + X is given by two components: one from 2P2F and one from 3P1F, via the observed Data and ZZ contribution;
- An usual expression for this procedure is:

Z + X at SR:

$$N_{SR}^{bkg} = (1 - \frac{N_{3P1F}^{ZZ}}{N_{3P1F}}) \sum_i N_{3P1F} \frac{f_a^i}{(1-f_a^i)} - \sum_j N_{2P2F} \frac{f_b^j}{(1-f_b^j)} \frac{f_c^j}{(1-f_c^j)}$$



- Sys. uncertainties from FR (due to difference on the bkg. composition at FR and CRs) is computed and propagated to the final Z + X estimation;
- OS-OS estimation validated by OS-SS cross-checking;
- Events selected in the two CRs were stored for training ANN and derive its Z + X shape;

m_{4l} Distributions and Yields

After SM Higgs Selections

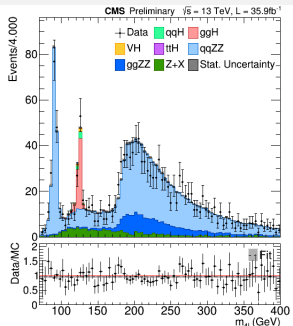


Table 16: Number of expected events from background and signal, with total (statistical+systematic) uncertainty reported, and number of observed events after the SM Higgs selections in the mass range $m_{4l} > 70 \text{ GeV}$.

| Process | 4μ | $4e$ | $2e2\mu$ | $4l$ |
|---------------------------------------|--------------------|--------------------|--------------------|---------------------|
| ggH | 19.34 ± 3.73 | 11.02 ± 2.34 | 25.99 ± 5.20 | 56.35 ± 6.81 |
| VH | 1.45 ± 0.21 | 0.92 ± 0.14 | 2.14 ± 0.32 | 4.51 ± 0.41 |
| ttH | 0.36 ± 0.08 | 0.23 ± 0.05 | 0.48 ± 0.11 | 1.07 ± 0.14 |
| qqZZ+ZZJJ | 387.01 ± 24.48 | 234.64 ± 24.81 | 538.35 ± 43.61 | 1160.00 ± 55.83 |
| ggZZ | 65.81 ± 7.43 | 43.85 ± 6.14 | 102.32 ± 12.60 | 211.98 ± 15.86 |
| Z+X | 24.28 ± 7.71 | 27.80 ± 8.09 | 56.90 ± 17.09 | 108.99 ± 20.42 |
| Σ backgrounds | 498.25 ± 26.98 | 318.46 ± 26.91 | 726.18 ± 48.78 | 1542.89 ± 61.90 |
| qqH (signal $m_H = 125 \text{ GeV}$) | 1.86 ± 0.36 | 1.10 ± 0.24 | 2.53 ± 0.52 | 5.49 ± 0.68 |
| Total expected | 500.11 ± 26.98 | 319.56 ± 26.91 | 728.71 ± 48.78 | 1548.38 ± 61.90 |
| Observed | 503 | 287 | 669 | 1459 |

After VBF-SR Selections

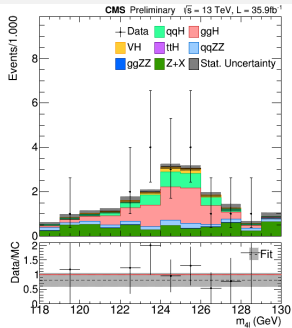


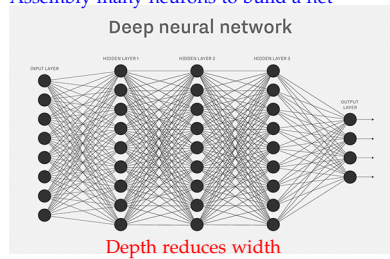
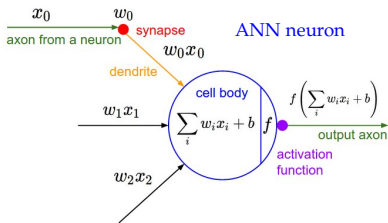
Table 17: Number of expected events from background and signal, with total uncertainty (statistical+systematic), and the number of observed events after the VBF-SR selections (see Sec. 4.3).

| Process | 4μ | $4e$ | $2e2\mu$ | $4l$ |
|---------------------------------------|-----------------|-----------------|-----------------|------------------|
| ggH | 2.46 ± 0.53 | 1.28 ± 0.30 | 3.10 ± 0.69 | 6.84 ± 0.92 |
| VH | 0.34 ± 0.05 | 0.20 ± 0.03 | 0.46 ± 0.07 | 1.00 ± 0.09 |
| ttH | 0.05 ± 0.01 | 0.03 ± 0.01 | 0.06 ± 0.01 | 0.14 ± 0.02 |
| qqZZ+ZZJJ | 0.67 ± 0.04 | 0.36 ± 0.04 | 0.74 ± 0.06 | 1.77 ± 0.08 |
| ggZZ | 0.05 ± 0.01 | 0.03 ± 0.01 | 0.06 ± 0.01 | 0.14 ± 0.02 |
| Z+X | 2.03 ± 0.83 | 0.33 ± 0.04 | 2.72 ± 0.76 | 5.08 ± 1.12 |
| Σ backgrounds | 5.60 ± 0.99 | 2.23 ± 0.31 | 7.14 ± 1.03 | 14.97 ± 1.46 |
| qqH (signal $m_H = 125 \text{ GeV}$) | 1.05 ± 0.22 | 0.58 ± 0.13 | 1.39 ± 0.30 | 3.02 ± 0.39 |
| Total expected | 6.65 ± 1.01 | 2.81 ± 0.34 | 8.53 ± 1.07 | 17.99 ± 1.51 |
| Observed | 5 | 2 | 10 | 17 |

Artificial Neural Networks (ANNs)

- Functionals coming from Machine Learning field (closest field to development of Artificial Intelligence) in Computer Science;
- ANNs have been successfully applied in many tasks as recognition of hand-written digits, images, sounds, sequences of data, play games, etc;
- Google and Microsoft are investing on them: Deep Mind, Cloud Machine Learning Engine, Cortana, Azure Studio, etc;
- An ANN is basically a function which the arguments are functions:
 $\Omega(x) = \Phi(f_1(x), f_2(x), \dots, f_n(x))$;
- It was inspired by neuron-science: how the brain works;

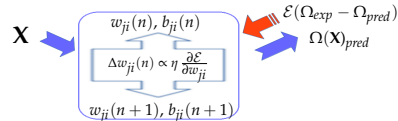
Assembly many neurons to build a net



Artificial Neural Networks (ANNs)

- Training an ANN consists in finding parameters (w_i and b_i) for $\Omega(x)$, such that it models a dataset in the best (possible) way;
- Supervised ANN training:
 - Present examples to ANN and their expected $\Omega(x)$ outputs;
 - Computes difference between expected and NN predictions;
 - Update w_i and b_i using this difference;
 - Repeat until predictions are good
- Here's an ANN learning $f(x) = a \cdot x + b$ (just a linear dataset):

enough (minimize the difference);



MC Preparation for ANN Training

- For the ANN studies the MCs¹ are prepared in the following way:
- The channels ($4e$, 4μ and $2e2\mu$ selected separately) are merged into just a sample for each MC (the channels are randomized inside the sample);
- Each merged sample are split into 2 independent sets:
 - **Training**: contains 80% of all events (from each sample) and is used to train ANNs;
 - **Testing**: contains remaining 20% of events and is used to test ANN after training;
- Then each set of all MCs are merged (and randomized) to compose the final training/testing input set to train/test ANNs;
- Additionally, two subsets have been defined based on the available number of jets per event:
 - **Njets2**: only events with exactly two jets;
 - **Njets3**: only events with at least three jets;
- ANNs are built and trained via the open-source **Keras**² (standard ML community tool) python package;

¹Data is not used on ANN training.

²<https://keras.io/> (now interfaced with TMVA).

Training Strategy

- It's hard to assure a set of parameters as the best one;
- ANN architecture optimization by scanning over several parameters;
- One ANN chosen for each Njets case via $\max(\epsilon.\pi)$ (ie. efficiency \times purity);

Training parameters (focus on low level variables)

| Parameter | Tested options |
|---------------------------|--|
| Inputs | leptons/jets(p_T, η, ϕ), MET |
| Pre-processing | none, normalization, standardization |
| Topologies ^a | 7:5:3, 21:13:8, 10:10:10:10, 30, 100, ... |
| Early stop ^b | 100, 600, 3000 |
| Minimizer ^c | SGD, Adam, Adagrad, Adadelta, RMSprop |
| Batch size ^d | 1, 5, 32, 64, 128, 786 |
| Neuron | ReLU, SeLU |
| Loss scaling ^e | XS (process total XS), $\sigma.\epsilon.BR$ (event weight) |
| Dropout ^f | none, 0.1, 0.3, 0.5, 0.7, 0.9, 0.99, 0.3:0.4:0.2, 0.5:0.25:0.1 |

^aThat refers to hidden layers. The output layer is always single sigmoid neuron

^bNumber of epochs to stop training if no improvement occurs.

^cMethod used to compute parameters update.

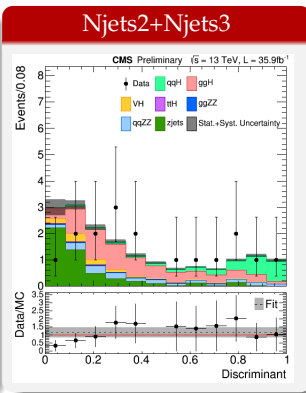
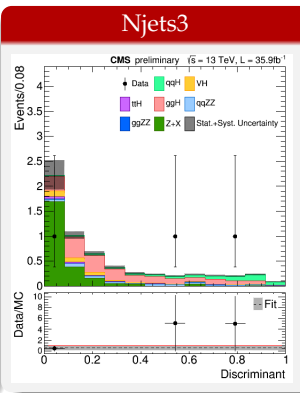
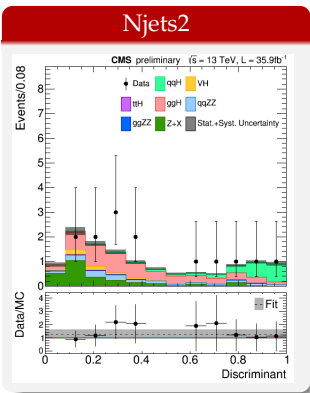
^dSubset from training set used to get parameters updates. N batches = N iterations per epoch.

^eIt's possible to use weights in training to optimize discrimination.

^fFraction of inputs randomly set to zero during training.

ANNs Shape for Njets2, Njets3 and their Combination

- Here are the (final) two ANNs chosen as VBF discriminants in each jet-based category and their combination;



- Z + X shape derived by feeding NNs with observed Data and ZZ MC³ and, repeating the procedure previously explained for this background estimation;

³Note that, the FR doesn't need to be redone.

Experimental and Theoretical Systematic Uncertainties

- Experimental and Theoretical systematic uncertainties accounted in this analysis (enter as log-normal nuisance parameters in the statistical analysis):

Experimental Uncertainties

| Source | Magnitude (%) |
|-----------------------------|---------------|
| Luminosity | 2.6 |
| Lepton $\epsilon_{ID/Reco}$ | 2.5-9 |
| Lepton energy scale | 0.04-0.30 |
| m_{4l} resolution | 20 |
| Jet energy scale | 3.3 |
| E_T^{miss} | 7-26 |
| b-tagging | 1 |
| Z + X | 6-23 |

Theoretical Uncertainties

| Source | Magnitude (%) |
|---|---------------|
| QCD scale (VBF) | +0.4/-0.3 |
| PDF set (VBF) | ± 2.1 |
| QCD scale (gg) | ± 3.9 |
| PDF set (gg) | ± 3.2 |
| Bkg K factor (gg) | ± 10.0 |
| QCD scale (WH) | +0.5/-0.7 |
| PDF set (WH) | ± 1.9 |
| QCD scale (ZH) | +3.8/-3.1 |
| PDF set (ZH) | ± 1.6 |
| QCD scale ($t\bar{t}H$) | +5.8/-9.2 |
| PDF set ($t\bar{t}H$) | ± 3.6 |
| QCD scale ($q\bar{q} \rightarrow ZZ$) | +3.2/4.2 |
| PDF set ($q\bar{q} \rightarrow ZZ$) | +3.1/-3.4 |
| Electroweak corrections ($q\bar{q} \rightarrow ZZ$) | ± 0.1 |
| $\text{BR}(H \rightarrow ZZ \rightarrow 4l)$ | 2.0 |

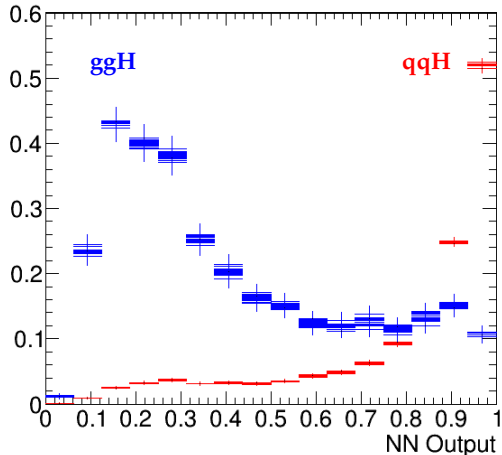
- The systematic uncertainties on the VBF ANN discriminants are added into the statistical analysis via their nominal and shifted shapes;

ANN Discriminants Systematic Uncertainties

- Systematic uncertainties on the ANN discriminants have been estimated from two sources: the systematic uncertainty on their inputs and the systematic uncertainty on the 3^{rd} jet;
- The first case (which affect both jet-based categories) the systematic uncertainty on the ANN discriminants shape and yield has been derived by feeding the discriminants with the $\pm 1\sigma$ shifted value of each input;
- The shifts are produced from one input variable at a time, such that, in the end there are $N_{(Inputs)} \times [1 + 2.N_{(InputsUncertainties)}]$ ANN distributions, including the nominal and shifted shapes;
- This procedure follows similar idea applied in previous CMS analysis:
 - cms.cern.ch/iCMS/jsp/openfile.jsp?tp=draft&files=AN2012_141_v9.pdf
 - <https://cds.cern.ch/record/2205282>
 - <https://cds.cern.ch/record/2273847>

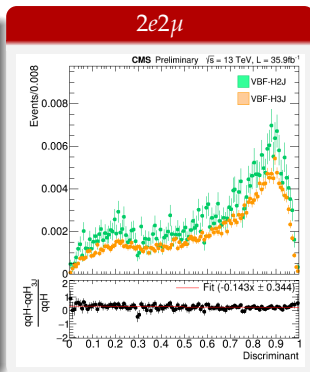
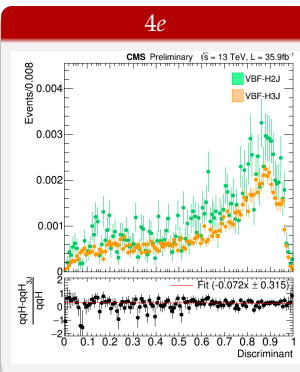
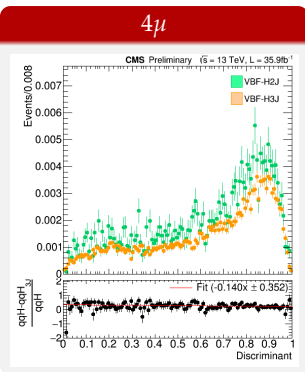
ANN Discriminants Systematic Uncertainties

- Here is an example of nominal and shifted distributions (superimposed) from one ANN for $\text{q}\bar{\text{q}}\text{H}$ and ggH (largest background) processes;
- The shifts look good and under control (in other words the discriminants are stable), mainly for the signal;



ANN Discriminants Systematic Uncertainties

- Since this analysis is proposing the usage of the 3rd jet and is not possible:
 - to replace the current VBF MC sample (VBF-H2J) by its NLO VBF-H3J version⁴;
 - or merge the two MC samples in suitable way;
- A systematic uncertainty⁵ because of using the 3rd jet from the current VBF MC sample has been estimated by computing the ratio between the ANN distribution using VBF-H2J and VBF-H3J, separately per four-lepton channel:



⁴Process VBF_HJJJ available at PowhegV2 (private generation following 2016 configurations).

⁵It affects only Njets3 category.

Statistical Analysis

- The statistical analysis is carried through Higgs Combine tool;
- A 1D binned shape analysis is performed on the VBF ANN discriminants, separately for each jet-based category and for their combination (using Combine tool);
- Inputs are the ANN discriminants via 1D histograms, containing the proper signal and background normalizations, along with the statistical and systematical uncertainties;
- Due to the low statistics of this analysis the HybridNew (fully Frequentist) method has been used (50k toys);
- Results achieved by combining the ANN discriminants from each jet-based category are highlighted in the next slides;

Statistical Analysis

- The VBF signal strength is measured to be $\mu \equiv \sigma_{qqH}^{Obs}/\sigma_{qqH}^{SM} = 1.28^{+1.24}_{-0.84}$ by combining ANN discriminants of Njets2 and Njets3 categories;

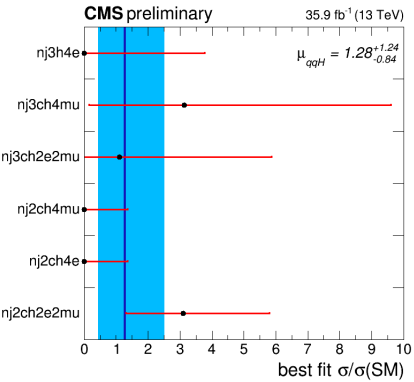
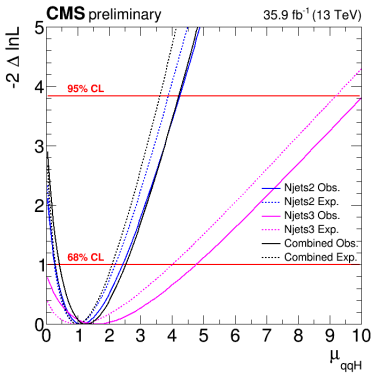
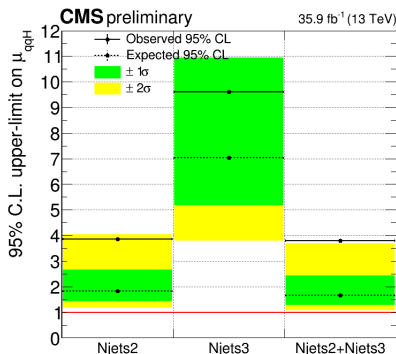
(g) μ_{qqH} likelihood scans.(h) μ_{qqH} best fit on each channel.

Table: Expected and observed signal strength modifiers from each category and four-lepton channel for 35.9fb⁻¹ of observed data at $\sqrt{s} = 13\text{TeV}$.

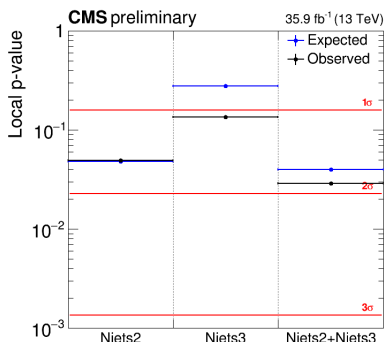
| Signal strength | $\mu_{qqH}^{4\mu,2J}$ | $\mu_{qqH}^{4e,2J}$ | $\mu_{qqH}^{2e2\mu,2J}$ | $\mu_{qqH}^{4\mu,3J}$ | $\mu_{qqH}^{4e,3J}$ | $\mu_{qqH}^{2e2\mu,3J}$ | $\mu_{qqH}^{4l,2J+3J}$ |
|-----------------|------------------------|------------------------|-------------------------|------------------------|------------------------|-------------------------|------------------------|
| Expected | $1.00^{+2.13}_{-1.49}$ | $1.00^{+3.11}_{-1.00}$ | $1.00^{+1.83}_{-0.96}$ | $1.00^{+5.79}_{-1.00}$ | $1.00^{+8.24}_{-1.00}$ | $1.00^{+4.67}_{-1.00}$ | $1.00^{+1.08}_{-0.70}$ |
| Observed | $0.00^{+1.36}_{-0.00}$ | $0.00^{+1.36}_{-0.00}$ | $3.10^{+2.69}_{-1.79}$ | $3.13^{+6.47}_{-2.98}$ | $0.00^{+3.78}_{-0.00}$ | $1.10^{+4.77}_{-1.14}$ | $1.28^{+1.24}_{-0.84}$ |

Statistical Analysis

- Limits and significances have been computed via the HybridNew method:
 - Limits show that hypothesis of VBF events in the present analysis can't be excluded, setting $\mu_{qqH}^{Obs} < 3.8$ and $\mu_{qqH}^{Exp} < 1.7$ at 95%CL;
 - Significances obtained are $\sigma_{qqH}^{Obs} = 1.9$ and $\sigma_{qqH}^{Exp} = 1.8$;



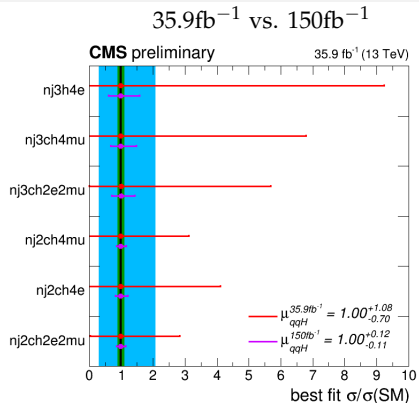
(i) Upper limits on μ_{qqH} .



(j) Significances via the present analysis.

Projections for Future Luminosities

- The VBF signal strength measurement and the significance of the present analysis has been projected for future luminosities scenarios at the LHC;
- Systematic uncertainties have been accounted by scaling the present luminosity;
- The total uncertainty on the measurement of μ_{qqH} is expected to reduce $\sim 87\%$ at $L = 150\text{fb}^{-1}$;



- Significance of 5.1σ is expected for a luminosity 10x larger than the present one;

Table: Comparison of the expected VBF significance between the present luminosity (35.9fb^{-1}) and future scenarios at the LHC.

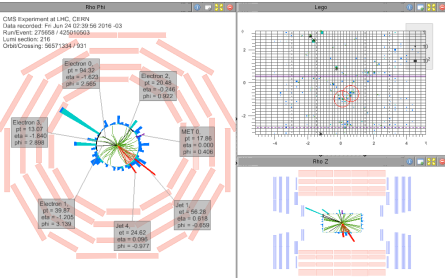
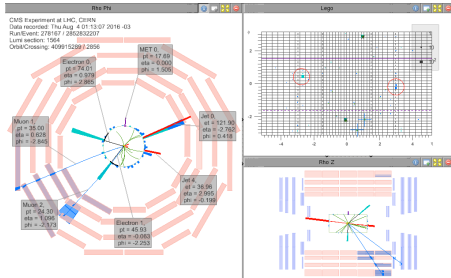
| Luminosity (fb^{-1}) | 35.9 | 150.0 | 300.0 | 359.0 | 1077.0 | 1795.0 | 3000.0 |
|--|------|-------|-------|-------|--------|--------|--------|
| Factor ($\times L^{35.9\text{fb}^{-1}}$) | 1.00 | 4.18 | 8.36 | 10.00 | 30.00 | 50.00 | 83.57 |
| Expected significance | 1.8 | 3.4 | 4.7 | 5.1 | 8.6 | 10.9 | 14.0 |

Most & Least VBF-Like Event Display in each Category

ANN score: 0.93

Njets2 Category

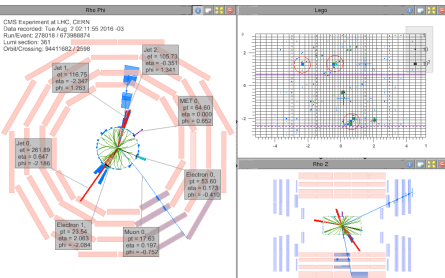
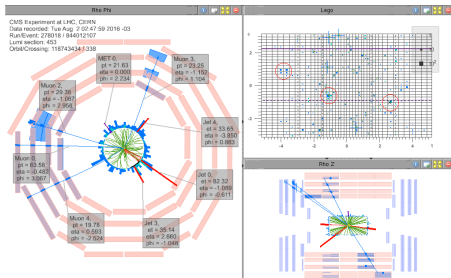
ANN score: 0.15



ANN score: 0.77

Njets3 Category

ANN score: 0.04



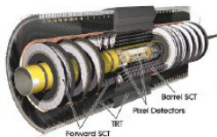
CMS Level 1 Tracking Trigger Associative Memory + FPGA

Introduction

- During his PhD the author was involved into the CMS Level 1 Tracking Trigger AM+FPGA project:
 - one of the three CMS-L1TT projects (CMS upgrade phase II - HLLHC):
 - Inclusion of inner-tracker data as part of L1 trigger;
 - Original tracker designed for $L_{inst.} \sim 10^{34} \text{ cm}^{-2} \cdot \text{s}^{-1}$ and PU_{Ave.} $\sim 20\text{-}30$;
 - Expected in phase II: $L_{inst.} \sim 10^{34} \text{ cm}^{-2} \cdot \text{s}^{-1}$ and PU_{Ave.} $\sim 140\text{-}200$;
 - Required decision time: $5\mu\text{s}$;
 - 500-1k Tb/s of data to be processed;
 - leaded by Fermilab working group;
 - the project aims for the usage of Associative Memories in combination with FPGAs;
 - the author studied and implemented new components on the available software:
 - synthetic match;
 - duplicate removal;
 - stub bending;
 - road and combination truncation
 - track fitter χ^2 adjustment;
 - results have been produced with different high-lumi scenarios (2-10k events):
 - $(\mu/\pi/e) + \text{PU}(140, 200, 300, 400)$;
 - $\nu + \text{PU}(140, 200, 250)$ (simulates pure PU, low p_T particles);
 - $t\bar{t} + \text{PU}200$;
 - jets($p_T = 250\text{GeV}$) + PU200;
 - hardware work: board inspections and tests;

The CMS-L1TT AM+FPGA Approach

Tracker Detector



Data transfer

**Data
formatting**

Partition detector into
trigger towers/sectors

Pick your favorite method:

*Associative Memory (AM) Approach
(proven approach from CDF/SVT)*

*Hough Transformation
tracklet-based*

Adaptive Pattern Recognition

*Biology Inspired ...
your choice here...*

**Pattern
Recognition**

Finer pattern recognition

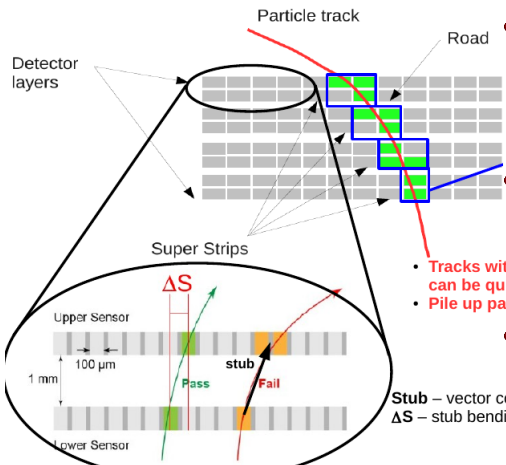
**Track
Fitting**

- The three CMS-L1TT projects can be divided into three stages:

- Data Formatting:** fragmentation of the CMS detector in $\eta - \phi$ sectors (trigger towers);
- Pattern Recognition:** selection of coarse hits patterns (potentially real tracks);
- Track Fitting:** extraction of refined track info using all hits from selected patterns;

The CMS-L1TT AM+FPGA Approach

- Here's the main idea and definitions adopted in the CMS L1TT AM+FPGA approach:
 - Superstrip (SS):** cluster of hits in the detector layers. They receive an ID based on their $z - \phi$ position;
 - Road:** pattern of built from SS's;



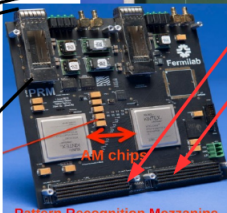
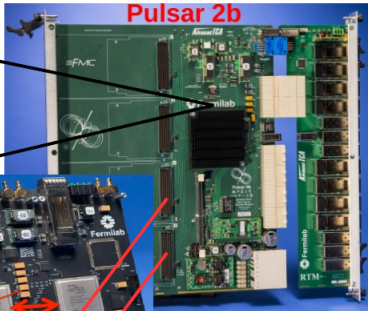
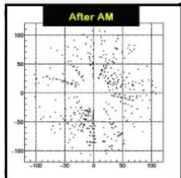
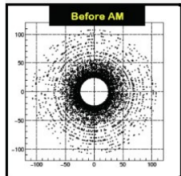
- An AM chip containing a big set of roads simulated via MC triggers the roads observed in real data. The hits from detector layers are processed in parallel;
- Once real roads are triggered, a set of possible hits combinations are built (possible tracks);
 - Tracks with pT below a threshold can be quickly rejected;
 - Pile up particles most $pT \leq 2\text{ GeV}$
- A fit select which combination is a real tracker;

Stub – vector connecting 2 sub-layers

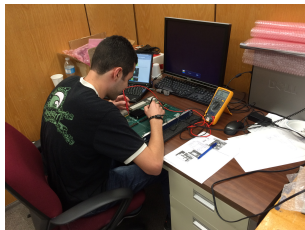
ΔS – stub bending (half strip cluster distance)

The Hardware for the CMS-L1TT AM+FPGA

Input: all hits from a collision

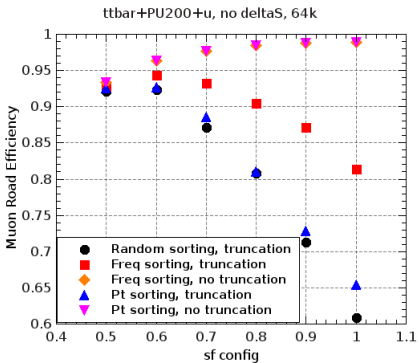


Output: useful tracks



Simulation Studies: Roads and Combinations Truncation

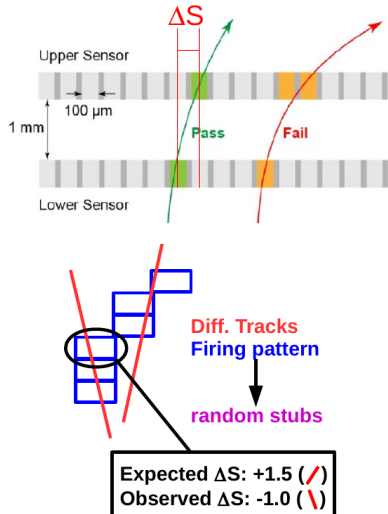
- It was needed to check the approach under truncation of roads and combinations (for reducing latency, for instance);
- Implemented two new flags into the software for controlling the number of roads and combinations to be accepted for further processing;
- A study done by the author showed the smallest impact on the efficiency due to truncation happens when roads are sorted by frequency:



Simulation Studies: Stub Bending (ΔS)

- The stub bending is the core idea behind the CMS L1TT project:
 - It helps to mitigate PU (mainly low p_T particles);
- In the AM+FPGA approach the ΔS prevents random patterns to be fired:
 - Without ΔS an AM pattern can be triggered by hits coming from different real tracks crossing the detector layers in different angles;
 - The ΔS was encoded in the AM framework via the SS ID's. The following formula defines the SS ID when the stub bending is required:

$$ss = i_{\Delta S} * N_\phi + i_\phi$$



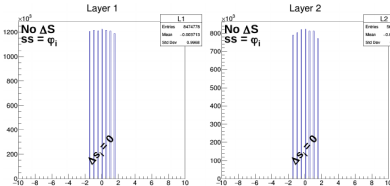
Simulation Studies: Stub Bending (ΔS)

- The SS- ΔS formula:

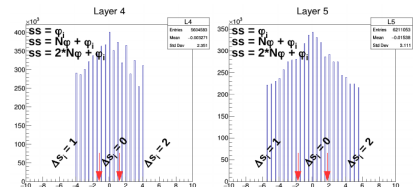
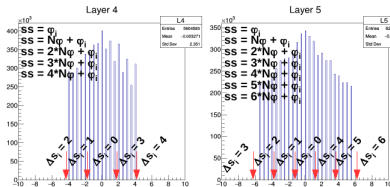
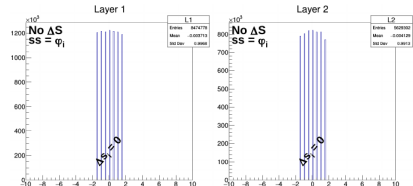
$$ss = i_{\Delta S} * N_{\phi} + i_{\phi}$$

- $i_{\Delta S}$: ΔS value of a given stub (max);
- N_{ϕ} : number of trigger-tower segmentations in ϕ ;
- i_{ϕ} : index of the ϕ segment which the stub belongs;
- Two possibilities of building the SS ID's according to the ΔS values:

Symmetric (eg. SYM115577)



Asymmetric (eg. ASYM115577)

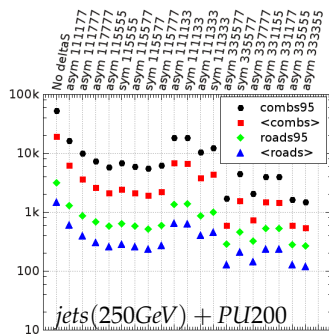
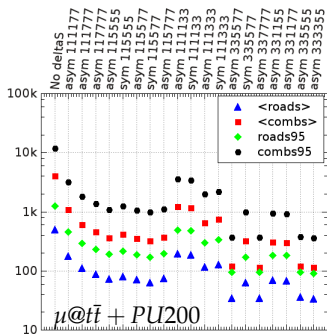


Simulation Studies: Stub Bending (ΔS)

- This ΔS approach allows the following schemes (negative ranges omitted):

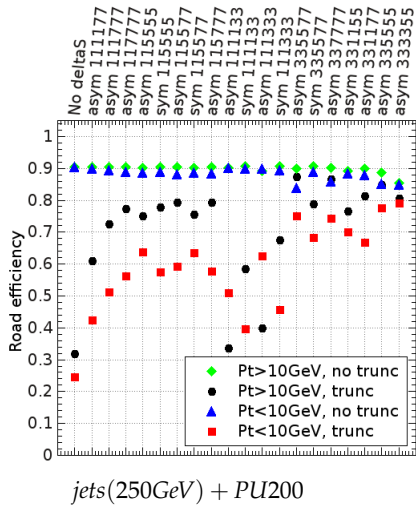
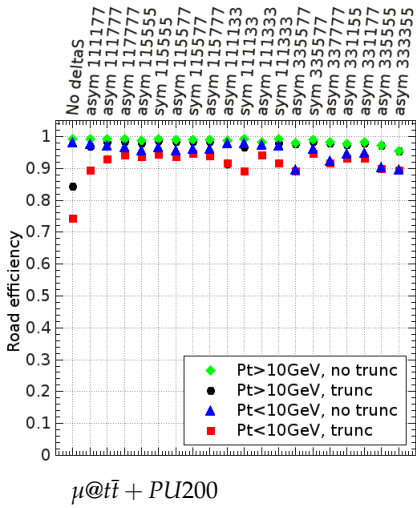
| #ranges | range width | ΔS values ([] central ranges) |
|---------|-------------|---|
| 3 | 9 | [-2.0, 2.0], [2.5, ...] |
| 5 | 7 | [-1.5, 1.5], [2.0, 5.5], [6.0, ...] |
| 7 | 5 | [-1.0, 1.0], [1.5, 3.5], [4.0, 6.0], [6.5, ...] |
| 9 | 3 | [-0.5, 0.5], [1.0, 2.0], [2.5, 3.5], [4.0, 5.0], [5.5, ...] |

- Effect of ΔS on the number of roads and combinations:
 - Reduction of up to $\sim 10x$ on roads and $\sim 50x$ on combinations;
 - Symmetric method produces few more combs/roads than Asymmetric one;



Simulation Studies: Stub Bending (ΔS)

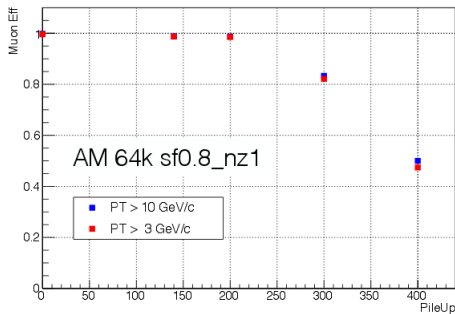
- Effect of ΔS on the road efficiency:
 - Up to 20% and 50% of efficiency can be recovered when truncation is applied;



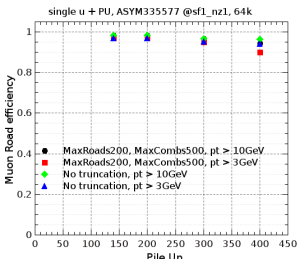
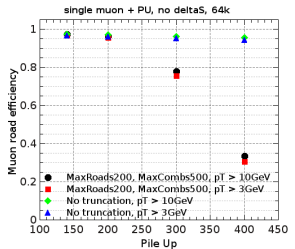
Simulation Studies: Stub Bending (ΔS) - The Edge of the Mountain

- At the ending of author's iteration with the CMS L1TT AM+FPGA there was a worry about PU spikes (as it happened in LHC Run I);
- Studies with single- μ +PU presented in the group showed large efficiency loss at very high PU:

Single muon + PileUP, AM = 64K, maxroads = 200, maxcombs = 500, HT8x8C

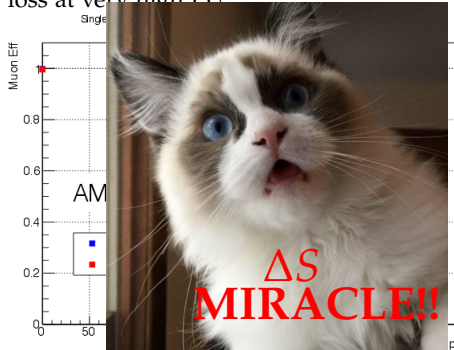


- The author decided to check that and apply the ΔS approach (not considered by them at that time):

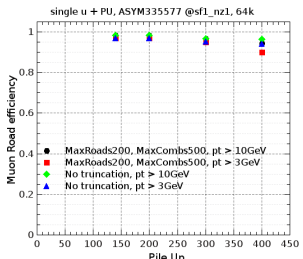
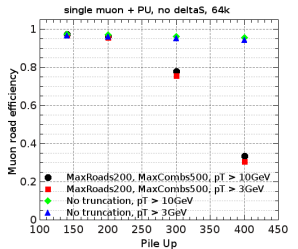


Simulation Studies: Stub Bending (ΔS) - The Edge of the Mountain

- At the ending of author's iteration with the CMS L1TT AM+FPGA there was a worry about PU spikes (as it happened in LHC Run I);
- Studies with single- μ +PU presented in the group showed large efficiency loss at very high PU;

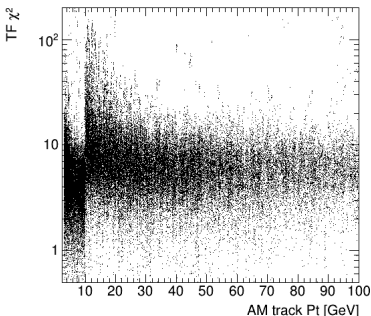


- The author decided to check that and apply the ΔS approach (not considered by them at that time):



Simulation Studies: χ^2 Revision

- In order to optimize the final results, it was decided to re-study the tracking fitter χ^2 value;
- It decides whether a combination of stubs is fine or not;
- Points to address:
 - Just an unique cut applied;
 - Dependence on the tracks p_T ;
- A new set of cuts have been adopted:
 - 6/6 combinations have a tight and unique threshold given by the 99% percentile of the theoretical $\chi^2_{ndof=8}$ curve (equals to 20.2);
 - 5/6 combinations have a p_T -based cut according to 8 ranges, which were defined to guarantee $\epsilon_{tracks}^{6/6+5/6} = 0.99 * \epsilon_{roads}^{6/6+5/6}$

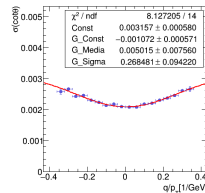
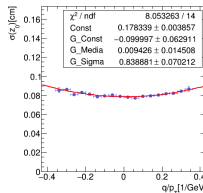
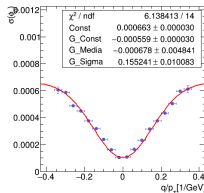
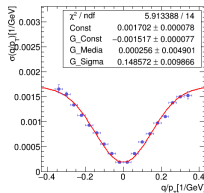


Simulation Studies: Synthetic Efficiency

- Synthetic efficiency is meant to check the efficiency based on the track parameters (q/p_T , ϕ_0 , z_0 and $\cot \theta$);
- Task: match MC and AM reco tracks using their parameters;
- For so, one defines a χ^2 -like function:

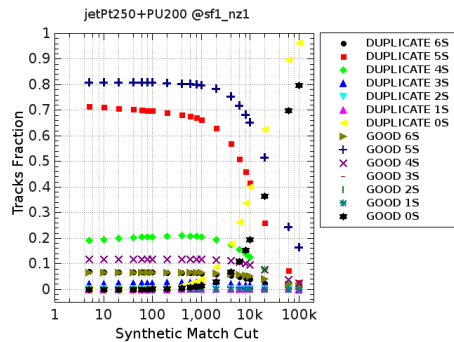
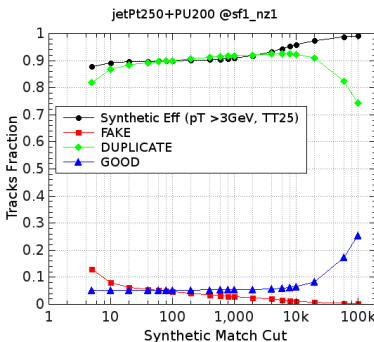
$$\chi^2_{match} = \sum_{i=0}^4 \frac{\delta^2 p_i}{\Omega^2(q/p_T)_i}, \quad \delta p_i = (p_i^{MC} - p_i^{Reco})$$

- The Ω function normalizes the dependence between the resolution in each track parameter and q/p_T :



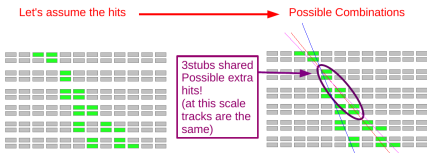
Simulation Studies: Synthetic Efficiency

- The χ_{match} establishes three types of tracks when receives a threshold value \bar{q} :
 - Good:** first reco track with smallest χ_{match} and $< \bar{q}$;
 - Duplicate:** other reco tracks with $\chi_{match} < \bar{q}$ but $\chi_{match} \geq \chi_{match}^{smallest}$;
 - Fake:** any reco track with $\chi_{match} \geq \bar{q}$;
- In order to define the value \bar{q} a tracking match based on stubs was carried out along with the synthetic efficiency:
 - Scanning the cut on χ_{match} one checks (on a dedicated MC sample) the number of original stubs present in the reco track;
 - Then, reduces the Fake rate and increases the Good rate as much as possible, avoiding random stub combinations (GOOD <5S) to pass the χ_{match} cut;
 - It was decided to have $\chi_{match} = 40$;



Simulation Studies: Duplicate Removal

- The pattern match based on SS clusters produces several duplicate tracks in the CMS L1TT AM+FPGA;
- For that reason, a procedure to remove such tracks has been developed: the duplicate removal;
- The duplicate removal is a stub-based mechanism:
 - A reco track is taken from the reco tracks list (**A**) and inserted on a new tracks list (**A'**);
 - Then, a loop is done over the remaining tracks on list **A**:
 - If a track is found to share a given number \bar{n} of stubs with any track on the list **B**, it is removed from list **A**;
 - Otherwise, the track is stored into the list **B**;
 - The tracks remaining in the list **B** are the final tracks;
- The DR mechanism was studied in order to tune the minimum number of stubs which allows massive remotion of duplicated tracks and keeps the track reco efficiency high;



Simulation Studies: Duplicate Removal

- Here are some results obtained for the DR tuning⁶;
- The final DR cut was chosen to be 0 (zero);

$\mu + PU200$

| DR option | Goods | Duplicates | Fakes | Track eff | Synthetic eff |
|-----------|-------|------------|-------|-----------|---------------|
| None | 1.976 | 25.785 | 0.614 | 0.985 | 0.989 |
| 5 | 1.976 | 25.785 | 0.614 | 0.985 | 0.989 |
| 4 | 1.976 | 8.898 | 0.275 | 0.98 | 0.989 |
| 3 | 1.973 | 0.604 | 0.095 | 0.964 | 0.989 |
| 2 | 1.969 | 0.065 | 0.047 | 0.953 | 0.989 |
| 1 | 1.967 | 0.007 | 0.039 | 0.951 | 0.988 |
| 0 | 1.966 | 0.000 | 0.038 | 0.951 | 0.988 |

$jet(p_T = 250GeV) + PU200$

| DR option | Goods | Duplicates | Fakes | Track eff | Synthetic eff |
|-----------|-------|------------|-------|-----------|---------------|
| None | 8.506 | 143.735 | 8.924 | 0.89 | 0.897 |
| 5 | 8.506 | 143.735 | 8.924 | 0.89 | 0.897 |
| 4 | 8.506 | 52.935 | 4.109 | 0.883 | 0.897 |
| 3 | 8.481 | 4.746 | 1.167 | 0.823 | 0.895 |
| 2 | 8.431 | 0.642 | 0.597 | 0.754 | 0.889 |
| 1 | 8.412 | 0.067 | 0.506 | 0.738 | 0.887 |
| 0 | 8.406 | 0.003 | 0.482 | 0.74 | 0.886 |

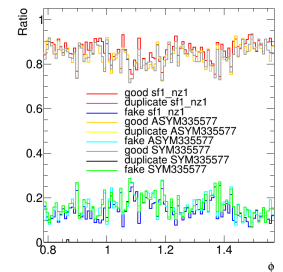
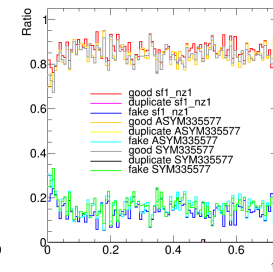
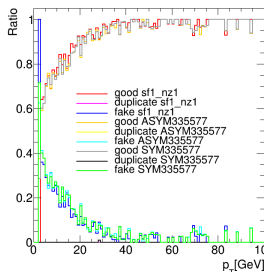
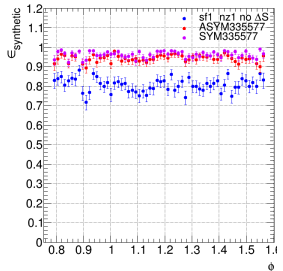
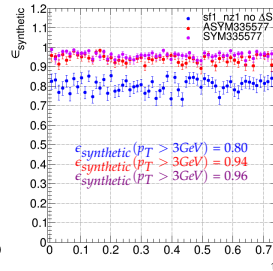
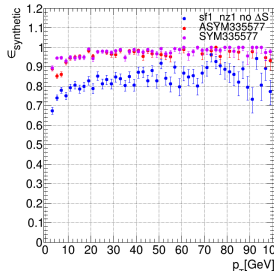
⁶ Notice the gap between the track and synthetic efficiencies: that comes from the extra stubs which builds up a good (stubs) combination for the original track

Simulation Studies: Final FOMs

- The next slides summarizes the final results found via the simulation package adopting the implementations presented here;
- The FOMs (figures of merit) are the common graphs used within the CMS L1TT AM+FPGA approach in order to show the performance of simulation studies;
- The FOMs are the efficiency and track categorization rates versus (p_T, η, ϕ) ;

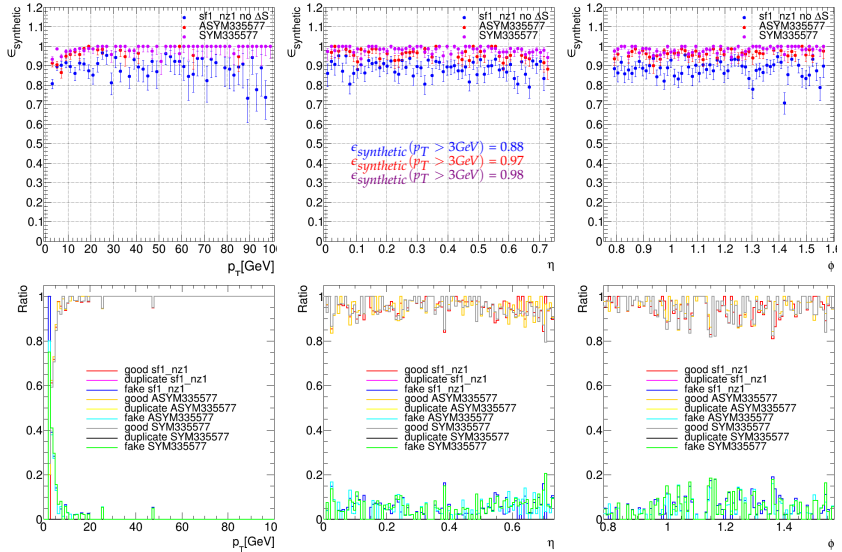
Simulation Studies: Final FOMs - μ in $t\bar{t} + PU200$

Figure: Track reconstruction efficiency for a μ in $t\bar{t} + PU200$ sample. The pattern bank used had 64k patterns and truncation at 200 roads and 500 combinations has been applied. Duplicate removal was applied by requiring DR=0.



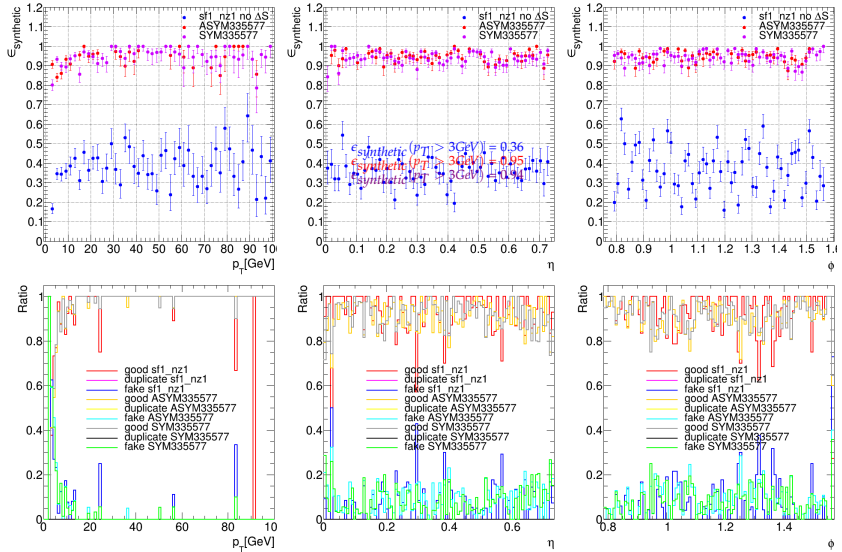
Simulation Studies: Final FOMs - $\mu + PU200$

Figure: Track reconstruction efficiency for $\mu + PU200$ sample. The pattern bank used had 64k patterns and truncation at 200 roads and 500 combinations has been applied. Duplication removal was applied by requiring DR=0.



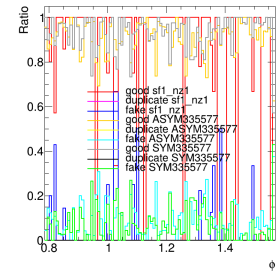
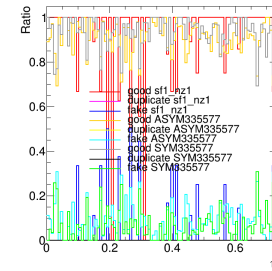
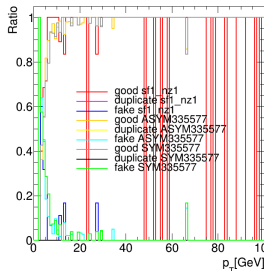
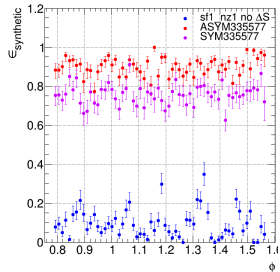
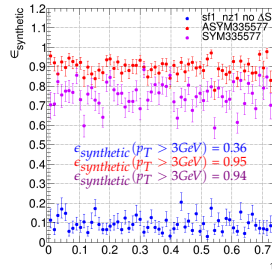
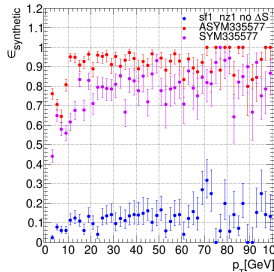
Simulation Studies: Final FOMs - $\mu + PU300$

Figure: Track reconstruction efficiency for $\mu + PU300$ sample. The pattern bank used had 64k patterns and truncation at 200 roads and 500 combinations has been applied. Duplication removal was applied by requiring DR=0.



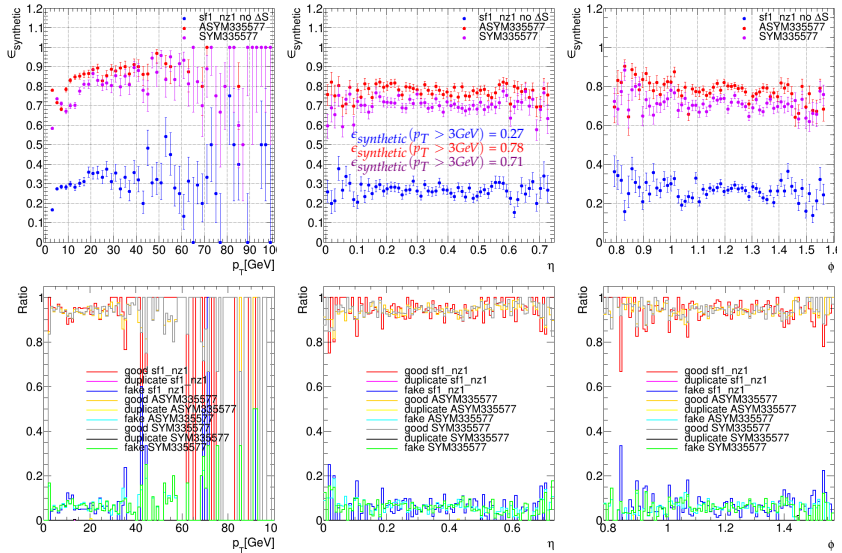
Simulation Studies: Final FOMs - $\mu + PU400$

Figure: Track reconstruction efficiency for $\mu + PU400$ sample. The pattern bank used had 64k patterns and truncation at 200 roads and 500 combinations has been applied. Duplication removal was applied by requiring DR=0.



Simulation Studies: Final FOMs - jets($p_T = 250\text{GeV}$) + PU200

Figure: Track reconstruction efficiency for jets($p_T = 250\text{GeV}$) + PU200 sample. The pattern bank used had 64k patterns and truncation at 200 roads and 500 combinations has been applied. Duplication removal was applied by requiring DR=0.



A Fast Matrix Element

Theoretical Foundation

- Here is presented a procedure called *Fast Matrix Element (FastME)*;
- It was studied in the very beginning of the author's PhD;
- The project was first idealized by prof(s). Andre Sznajder (DFNAE-UERJ) and Stephen Mrenna (CSD - FNAL):
 - A method capable of deriving event weight from MC sampling into a given phase space;
 - It should allow one to get proper normalization of random events, for instance;

Why Fast?

Table: Time to compute the weight of one event using *MadWeight5* (for an usual analysis these numbers multiplies by thousand).

| Process | Time/Event (s) |
|----------------------------|----------------|
| ZH | <5 |
| $t\bar{t}$ fully-leptonic | 10 |
| Zbb | 18 |
| $t\bar{t}$ semi-leptonic | 41 |
| $t\bar{t}H$ fully-leptonic | 60 |

ME Methods

$$\mathcal{P}(x|\alpha) = \frac{1}{\sigma_\alpha} \int d\omega_1 d\omega_2 f(\omega_1)f(\omega_2) \int d\Phi(y) |\mathcal{M}_\alpha(y)|^2 W(x,y)$$

- $\mathcal{P}(x|\alpha)$: an event probability;
- σ_α : process cross-section;
- $d\Phi$: analysis/detector acceptance;
- $f(\omega_i)$: Parton Distribution Function;
- $\mathcal{M}_\alpha(y)$: matrix element;
- $W(x,y)$: transfer function;

Theoretical Foundation

- The original idea of finding event weights didn't lead to promising results: assigned weights didn't model properly the events;
- A new idea appeared, then:
 - Would it be possible to discriminate events based on a match between the particles from a probe event and a MC one?
- *FastME* algorithm:
 - 1 Loop over the particles (i) from a MC event and match them to the particles (j) from a probe event according to

$$R_{(i,j)}^2 = \sum_{k=1}^n \left(\frac{v_k^{(i,MC)} - v_k^{(j,Data)}}{\sigma_{v_k}} \right)^2 \quad (1)$$

where, k stands for the kinematic variables (p_T , η , ϕ) and the particles pairs (i, j) are chosen to minimize $R_{i,j}$;

- 2 A distance between the probe event and the MC event is computed by summing in quadrature the minimum distances ($R_{i,j}$) between their particles:

$$D^2 = \sum_{i=1}^m [R_{(i,j)}^2]_{min}, \text{ with } j(i+1) \neq j(i) \quad (2)$$

- 3 Finally, a discriminant for the probe event is computed using the closest MC events (from each class) via the formulas

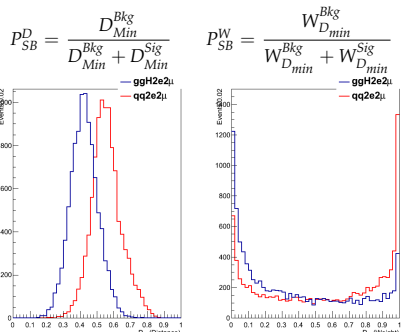
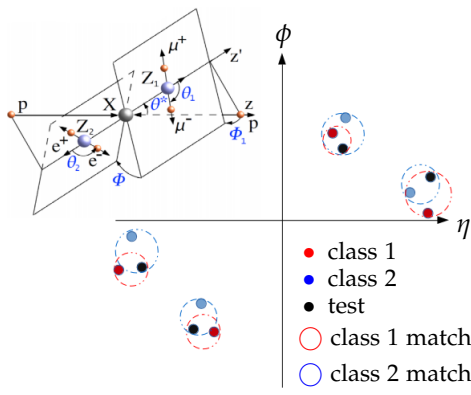
$$P_{SB}^D = \frac{D_{Min}^{Bkg}}{D_{Min}^{Bkg} + D_{Min}^{Sig}} \quad (3)$$

$$P_{SB}^W = \frac{W_{D_{min}}^{Bkg}}{W_{D_{min}}^{Bkg} + W_{D_{min}}^{Sig}} \quad (4)$$

Theoretical Foundation

- Here's an illustration of the method to clarify the algorithm:

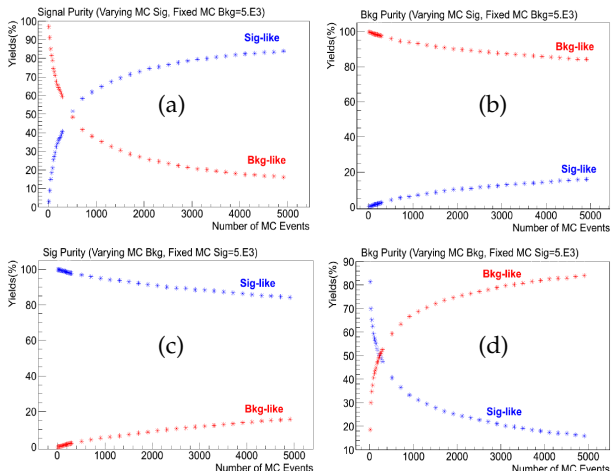
Figure: The MC events present a topology associated to the EM of a given physical process, such as, each particle has a correlation with the other particles in the event. A data event (black points) receives a probability of being from a kind or other (blue and red point) via the correlation of the distances (represented by the blue and red circles) between it and the MC events.



Simulation Studies: Bias from Pattern Bank Size

- The first point addressed during the development of the project was the influence of the pattern banks size:

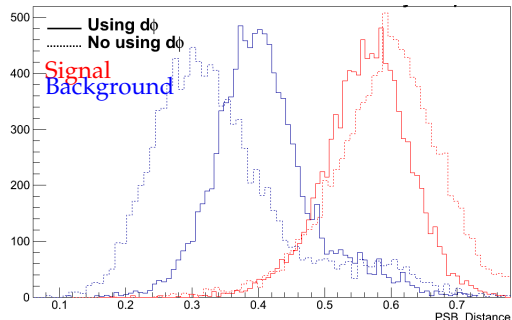
Figure: On graphs (a) and (b) the background pattern bank has a fixed size while the signal one is varied. On graphs (c) and (d) the opposite case is shown. Note, here "purity" is computed using the absolute number of events (without normalization).



Simulation Studies: Impact of ϕ Variable

- Some studies have been done in order to optimize the performance of the discriminants;
- In the beginning of the project results showed that ϕ and E (energy) doesn't contribute and can actually worse the discriminant performance;
- Below is a comparison between the P_{SB}^D distribution using ϕ and without it;
- Based on such plot ϕ was removed from the default algorithm within *FastME* and left as an option to the user;

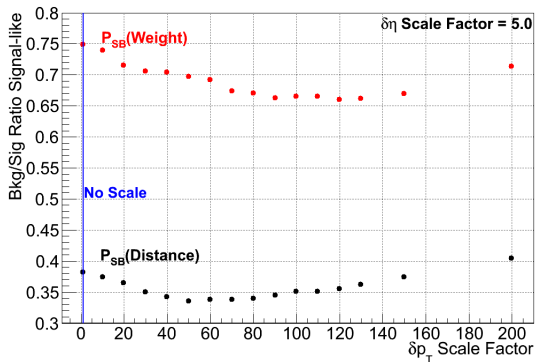
Figure: Impact on the P_{SB}^D distribution for signal and background due to use or not of ϕ in the computation of the distances between particles and events.



Simulation Studies: Scaling v_k 's Contribution

- Another point of optimization was the scaling of the variables used to compute the $R_{(ij)}$;
- Since the variables v_k present quite different ranges of variation it's important do level them:

Figure: Dependency on the variation of the fraction of signal events being mis-classified as background in function of the δp_T . A fixed value of 5.0 was used as the $\delta\eta$.

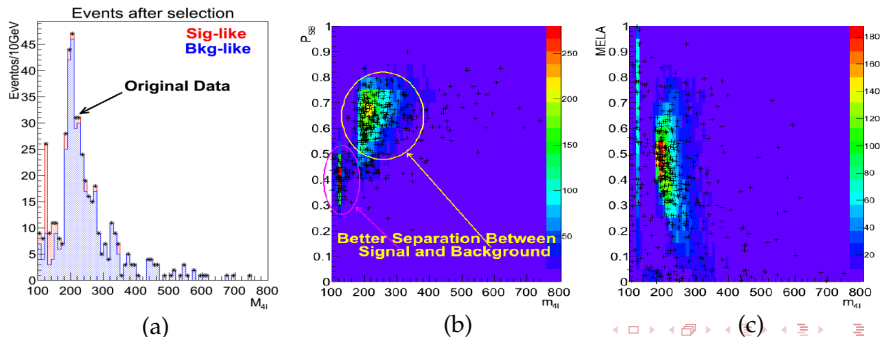


- The latest version of the project has an automated method which assigns the cumulative mean of MC events as the scaling factors;

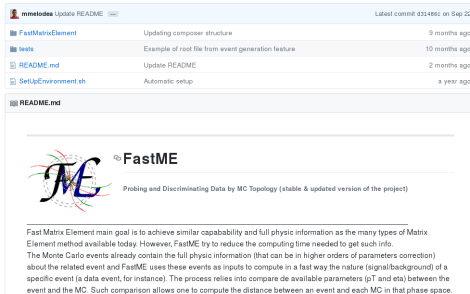
Simulation Studies: *FastME* Applied to HZZ4L CMS Data

- After interesting results with MadGraph/Powheg/Sherpa samples of ggH and qqZZ, it was natural an interest of applying *FastME* to the HZZ4L data collected by CMS on 2015 during the LHC RunI;
- The results have been compared to the formal CMS discriminant, the so called MELA;

Figure: (a) Observed events classified as signal and background by the *FastME*, (b) P_{SB}^D and (c) MELA discriminants distribution versus the m_{4l} .



The *FastME* Package



A screenshot of a GitHub repository page for 'FastMatrixElement'. The repository has 1 star and 1 branch. The README file is shown with the following content:

```
Fast Matrix Element main goal is to achieve similar capability and full physic information as the many types of Matrix Element method available today. However, FastME try to reduce the computing time needed to get such info. The Monte Carlo events already contain the full physic information (that can be in higher orders of parameters correction) about the related event and FastME uses these events as inputs to compute in a fast way the nature (signal/background) of a specific event (a data event, for instance). The process relies into compare de available parameters (pT and eta) between the event and the MC. Such comparison allows one to compute the distance between an event and each MC in that phase space.
```

- The success of *FastME* idea on real CMS data encouraged us to move the standalone codes created until that moment into a organized package;
- During the author's first travel to Fermilab, this package was created and stored on GitHub:

CONCLUSIONS

Conclusions

- ANN approach successfully implemented for an isolated VBF $H \rightarrow ZZ \rightarrow 4l$ XS measurement;
- Reliable procedure implemented for systematic uncertainties;
- Results provided from the combination of our best ANN configurations:
 - best fit for signal strength: $\mu_{qqH}^{Exp} = 1.00^{+1.08}_{-0.70}$ and $\mu_{qqH}^{Obs} = 1.28^{+1.24}_{-0.84}$;
 - 95%CL upper limits on μ_{qqH} : $\mu_{qqH}^{Exp} < 1.66$ and $\mu_{qqH}^{Obs} < 3.79$;
 - significances: $\sigma_{qqH}^{Exp} = 1.8$ and $\sigma_{qqH}^{Obs} = 1.9$;
- Projections provided for future luminosity scenarios at the LHC:
 - Expected to improve signal strength precision up to $\sim 87\%$ at the end of RunII;
 - Significance evolution:
- Analysis documentation is ready and released: [AN-18-120](#);

| Luminosity (fb^{-1}) | 35.9 | 150.0 | 300.0 | 359.0 | 1077.0 | 1795.0 | 3000.0 |
|--------------------------|------|-------|-------|-------|--------|--------|--------|
| Factor | 1.00 | 4.18 | 8.36 | 10.00 | 30.00 | 50.00 | 83.57 |
| Expected significance | 1.8 | 3.4 | 4.7 | 5.1 | 8.6 | 10.9 | 14.0 |

Conclusions

- **Ongoing:** analysis of full **2017 MC & Data**:

- package of macros for future studies (parallel ANN training, Z+X derivation and statistical analysis);
- already in use by a colleague in Bari (Nicola's student).

8 commits 1 branch 0 releases 1 contributor

Branch: **master** ▾ New pull request Find file Clone or download ▾

| | | |
|--|---|-----------------------------------|
|  mamelodea | updating guide for setting up keras at RECAS | Latest commit c37e05d 14 days ago |
|  Guide | updating guide for setting up keras at RECAS | 14 days ago |
|  Keras | Updating macros for Bari | 17 days ago |
|  StatisticalAnalysis | Initiating repository for CMS AN-18-120 codes | a month ago |
|  ZplusX | Initiating repository for CMS AN-18-120 codes | a month ago |
|  README.md | Initial commit | a month ago |

README.md

CMS_18_120_ANCodes

Macros from CMS AN-18-120



68 / 81



Datasets used in the Analysis

| Run range | Datasets | Integrated luminosity |
|---------------|---|------------------------|
| 273150-275376 | Global Tag: 80X_dataRun2_2016SeptRepro_v7 /DoubleMuon/Run2016B-03Feb2017_ver2-v2/MINIAOD /DoubleEG/Run2016B-03Feb2017_ver2-v2/MINIAOD /MuonEG/Run2016B-03Feb2017_ver2-v2/MINIAOD /SingleMuon/Run2016B-03Feb2017_ver2-v2/MINIAOD /SingleElectron/Run2016B-03Feb2017_ver2-v2/MINIAOD | 5.892 fb ⁻¹ |
| 275656-276283 | /DoubleMuon/Run2016C-03Feb2017_v1/MINIAOD /DoubleEG/Run2016C-03Feb2017_v1/MINIAOD /MuonEG/Run2016C-03Feb2017_v1/MINIAOD /SingleMuon/Run2016C-03Feb2017_v1/MINIAOD /SingleElectron/Run2016C-03Feb2017_v1/MINIAOD | 2.646 fb ⁻¹ |
| 276315-276811 | /DoubleMuon/Run2016D-03Feb2017_v1/MINIAOD /DoubleEG/Run2016D-03Feb2017_v1/MINIAOD /MuonEG/Run2016D-03Feb2017_v1/MINIAOD /SingleMuon/Run2016D-03Feb2017_v1/MINIAOD /SingleElectron/Run2016D-03Feb2017_v1/MINIAOD | 4.353 fb ⁻¹ |
| 276831-277420 | /DoubleMuon/Run2016E-03Feb2017_v1/MINIAOD /DoubleEG/Run2016E-03Feb2017_v1/MINIAOD /MuonEG/Run2016E-03Feb2017_v1/MINIAOD /SingleMuon/Run2016E-03Feb2017_v1/MINIAOD /SingleElectron/Run2016E-03Feb2017_v1/MINIAOD | 4.117 fb ⁻¹ |
| 277932-278808 | /DoubleMuon/Run2016F-03Feb2017_v1/MINIAOD /DoubleEG/Run2016F-03Feb2017_v1/MINIAOD /MuonEG/Run2016F-03Feb2017_v1/MINIAOD /SingleMuon/Run2016F-03Feb2017_v1/MINIAOD /SingleElectron/Run2016F-03Feb2017_v1/MINIAOD | 3.186 fb ⁻¹ |
| 278820-280385 | /DoubleMuon/Run2016G-03Feb2017_v1/MINIAOD /DoubleEG/Run2016G-03Feb2017_v1/MINIAOD /MuonEG/Run2016G-03Feb2017_v1/MINIAOD /SingleMuon/Run2016G-03Feb2017_v1/MINIAOD /SingleElectron/Run2016G-03Feb2017_v1/MINIAOD | 7.721 fb ⁻¹ |
| 281207-284068 | Global Tag: 80X_dataRun2_Prompt_v16 /DoubleMuon/Run2016H-03Feb2017_ver2-v1/MINIAOD /DoubleEG/Run2016H-03Feb2017_ver2-v1/MINIAOD /MuonEG/Run2016H-03Feb2017_ver2-v1/MINIAOD /SingleMuon/Run2016H-03Feb2017_ver2-v1/MINIAOD /SingleElectron/Run2016H-03Feb2017_ver2-v1/MINIAOD /DoubleMuon/Run2016H-03Feb2017_ver3-v1/MINIAOD /DoubleEG/Run2016H-03Feb2017_ver3-v1/MINIAOD /MuonEG/Run2016H-03Feb2017_ver3-v1/MINIAOD /SingleMuon/Run2016H-03Feb2017_ver3-v1/MINIAOD /SingleElectron/Run2016H-03Feb2017_ver3-v1/MINIAOD | 8.857 fb ⁻¹ |

JETMET POG Filters

| Filter | Description |
|--|---|
| HBHENoiseFilter HBHENoiseIsoFilter | remove noisy events from the HCAL, where the HBHE scintillator produces anomalous signals with pulse shapes and pixel multiplicities discrepant from those from a clean signal |
| EcalDeadCellTriggerPrimitiveFilter | removes events with non-functioning ECAL data links, comparing the sum of energy deposited in each supercluster cell to the energy saturation of the trigger primitive |
| goodVertices | filter events with noisy vertex reconstruction (due to pileup effects) by requiring the reconstruction of at least one good vertex full filling the following criteria: high number of degree of freedom ($NPV > 4$), collisions restricted along the zaxis ($zPV < 24\text{cm}$) and small radius of the PV ($rPV < 2\text{cm}$) |
| eeBadScFilter | removes events with noisy ECAL endcap superclusters |
| globalTightHalo2016Filter | removes events with enhanced MET from beam-halo particles which are in time with the beam |
| BadPFMuonFilter BadChargedCandidateFilter | remove events with mis-reconstructed muon and charged hadron PF candidates |

Post-Fit Yields and Distributions

Table 19: Background and signal estimations, with total uncertainty (statistical+systematic), derived from fitting the **s+b** model to the observed data, accounting 35.9fb^{-1} at $\sqrt{s} = 13\text{TeV}$.

| Process | 4μ | $4e$ | $2e2\mu$ | $4l$ |
|-------------------------------------|-----------------|-----------------|-----------------|------------------|
| ggH | 2.48 ± 0.34 | 1.29 ± 0.19 | 3.14 ± 0.44 | 6.91 ± 0.59 |
| VH | 0.34 ± 0.03 | 0.20 ± 0.02 | 0.46 ± 0.04 | 1.00 ± 0.06 |
| ttH | 0.05 ± 0.01 | 0.03 ± 0.00 | 0.06 ± 0.01 | 0.14 ± 0.01 |
| qqZZ+ZZJJ | 0.67 ± 0.04 | 0.36 ± 0.03 | 0.75 ± 0.05 | 1.77 ± 0.07 |
| ggZZ | 0.05 ± 0.01 | 0.03 ± 0.00 | 0.06 ± 0.01 | 0.14 ± 0.01 |
| Z+X | 1.74 ± 0.34 | 0.29 ± 0.06 | 2.35 ± 0.44 | 4.37 ± 1.34 |
| Σ backgrounds | 5.34 ± 0.49 | 2.19 ± 0.20 | 6.81 ± 0.63 | 14.34 ± 0.82 |
| qqH (signal $m_H = 125\text{GeV}$) | 1.35 ± 0.77 | 0.76 ± 0.42 | 1.79 ± 1.01 | 3.90 ± 1.34 |
| Total estimated | 6.69 ± 0.91 | 2.95 ± 0.47 | 8.60 ± 1.19 | 18.24 ± 1.57 |

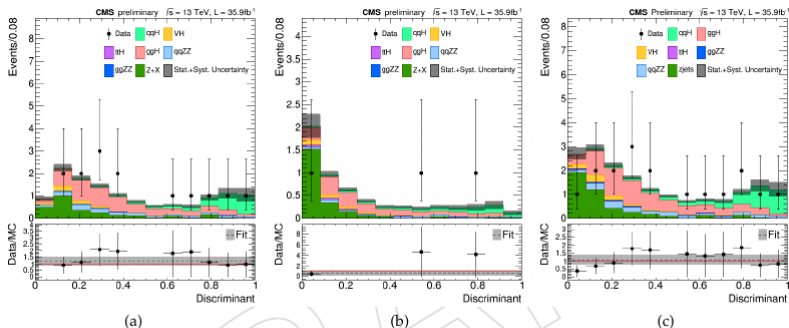
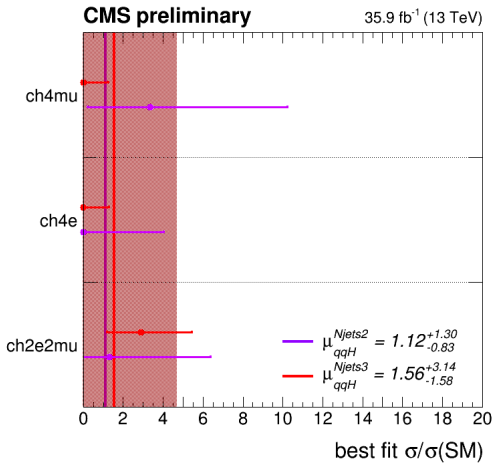


Figure 27: Post-fit NN distribution. The fit is done with the assumption of S+B hypothesis ($\mu_{VBF} = 1$ a priori).

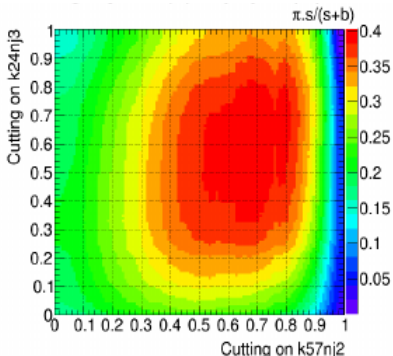
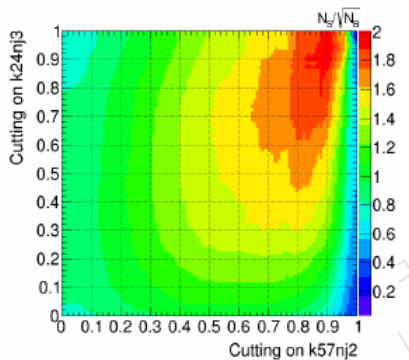
Comparison Between Best Fits of Njets2 and Njets3 Categories

- The best fits from each jet-based category. As it is shown, there's no advantage in using them alone instead of combining as it was done in the analysis;

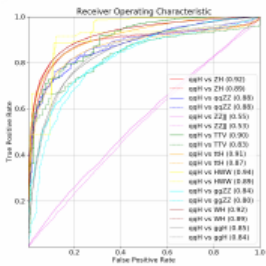
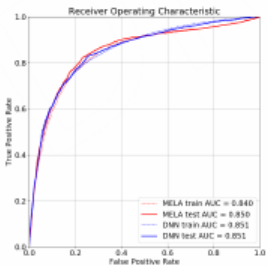
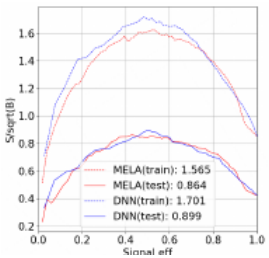
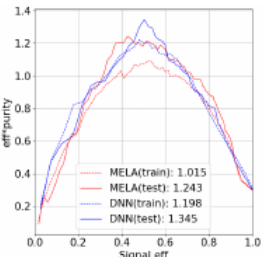
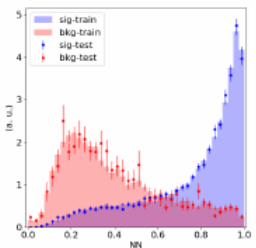
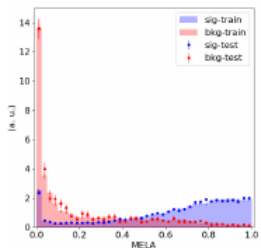


Sensitivity of Combined ANNs

- Note that, no systematic uncertainty has been accounted here;



ANNs Validation Plots



Events after SM Higgs Selections in each 4l Channel

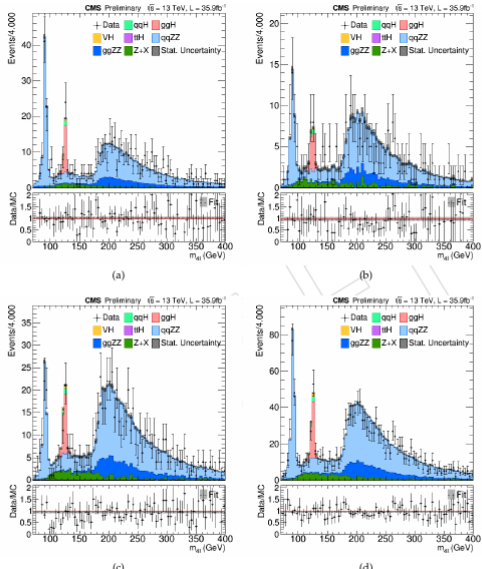
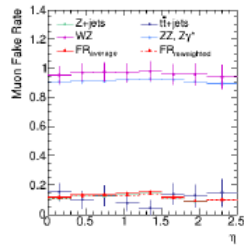
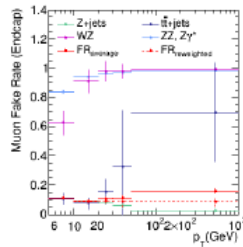
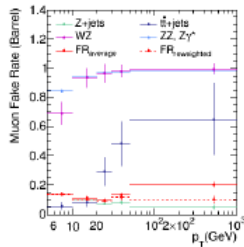
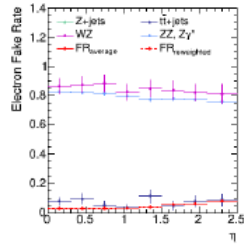
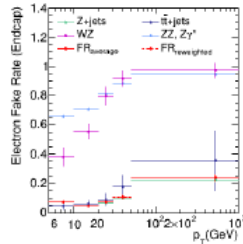
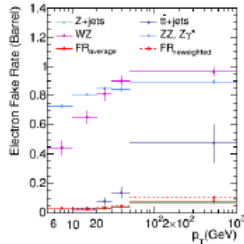


Figure 23: Final four-lepton mass distributions for the SM Higgs separated in the channels (a) 4μ , (b) $4e$ and (c) $2e2\mu$ and, combined into the (d) $4l$ final state. The distributions are shown for $70 < m_{4l} < 400$ GeV and include the $Z + X$ background estimated by the data-driven method explained in Sec. 6.4.

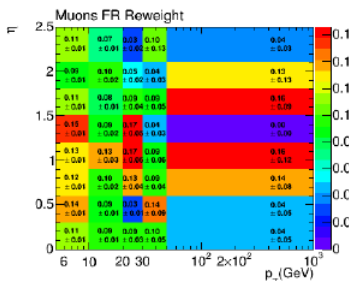
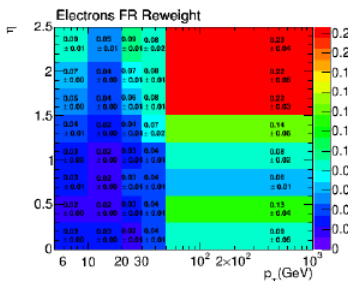
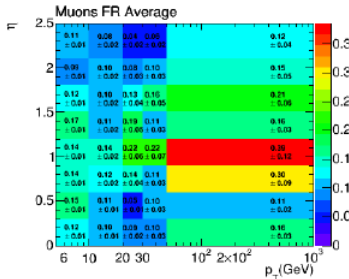
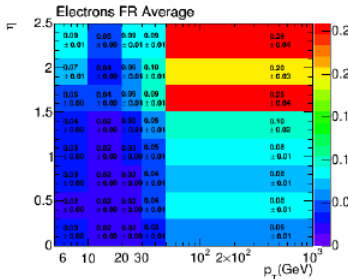
Z+X Systematic Uncertainty and Final Yields

- Z+X systematic uncertainty from FR: compute its variation by averaging MC ($DY, ZZ/Z\gamma, WZ, t\bar{t}$) FR and reweighing with 2P2F yields. Then propagate to Z+X estimation;



Z+X Systematic Uncertainty and Final Yields

- The behavior in 2D:

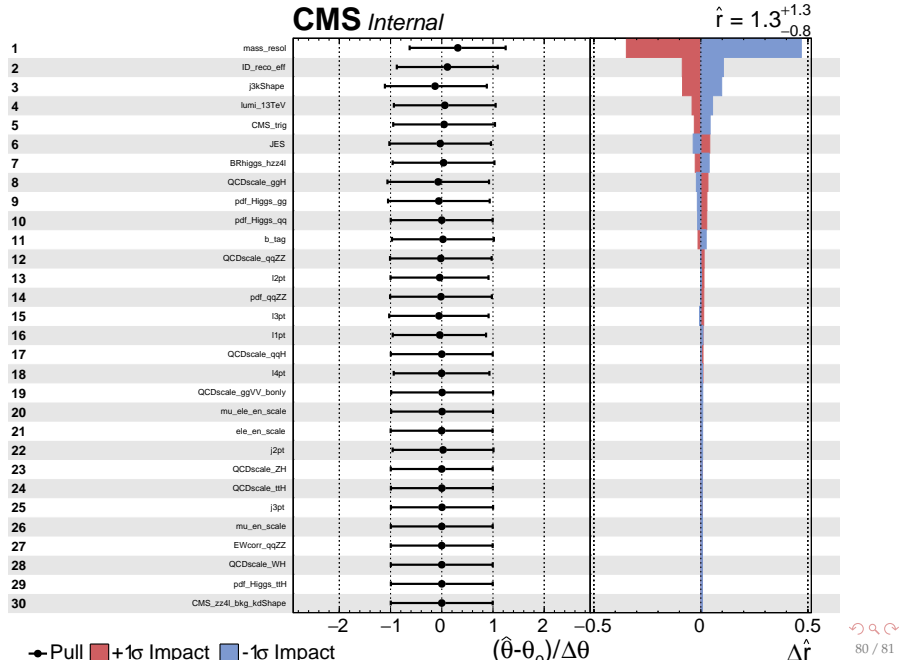


Z+X Systematic Uncertainty and Final Yields

Table 13: Final yields estimated for Z+X in the signal region from the measurements on data using the fake rate methods of opposite-sign (OS-OS) and same-sign (OS-SS) leptons. The estimates are reported with the total uncertainty for each final state after the SM Higgs and VBF-SR selections. The m_{4l}^{OS}/m_{4l}^{SS} is the ratio between the m_{4l} distribution for each final state obtained for Z+X in the OS and SS procedures (it is not computed for VBF-SR due to the very few Z+X events estimated there).

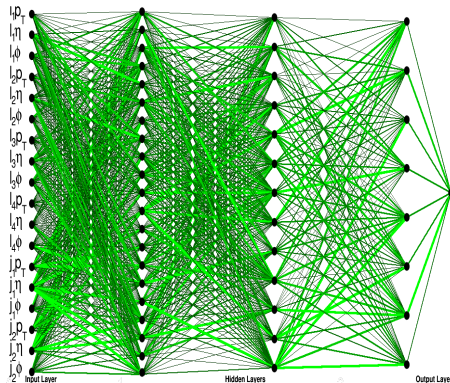
| Z+X | 4μ | 4e | $2e2\mu$ | 4l |
|---------------------------|------------------|------------------|------------------|--------------------|
| | | SM Higgs | | |
| OS-OS | 24.28 ± 7.79 | 27.80 ± 1.84 | 56.90 ± 6.71 | 108.99 ± 10.33 |
| OS-SS | 24.00 ± 4.90 | 36.00 ± 6.00 | 64.00 ± 8.00 | 124.00 ± 11.14 |
| m_{4l}^{OS}/m_{4l}^{SS} | 0.75 ± 0.31 | 0.88 ± 0.33 | 0.98 ± 0.35 | 0.85 ± 0.33 |
| | | VBF-SR | | |
| OS-OS | 2.03 ± 0.49 | 0.33 ± 0.20 | 2.72 ± 0.42 | 5.08 ± 0.68 |
| OS-SS | 1.00 ± 1.00 | 1.00 ± 1.00 | 0.00 ± 0.00 | 2.00 ± 1.41 |

Systematic Uncertainties Impact on μ_{qqH} Fit

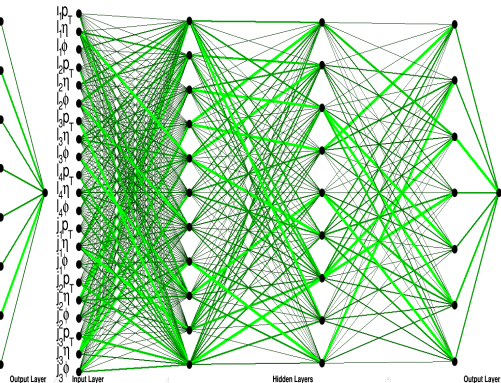


Architecture of Chosen ANNs

Figure: ANNs architecture created in this analysis. Black dots stand for inputs/neurons, while lines stand for the size of the ANN parameters chosen after training them. Wider and brighter lines means the parameter (weight or bias) associated to a given input for a neuron is larger (in other words its contribution is more relevant). ANN for Njets2 has 21:13:8 hidden neurons, while for Njets3 it has 11:9:7 (all neurons of SeLU type).



(a) Njets2 - 21:13:8



(b) Njets3 - 11:9:7